Design, Manufacturing, and Locomotion Studies of Ambulatory Micro-Robots

Design, Manufacturing, and Locomotion Studies of Ambulatory Micro-Robots

A dissertation presented

by

Andrew Thomas Baisch

to

The School of Engineering and Applied Sciences

in partial fulfillment of the requirements

for the degree of

Doctor of Philosophy

in the subject of

Engineering Sciences

Harvard University

Cambridge, Massachusetts

April 2013

Dissertation Advisor:

Professor Robert J. Wood

Author:

Andrew Thomas Baisch

Design, Manufacturing, and Locomotion Studies of Ambulatory Micro-Robots

Abstract

Biological research over the past several decades has elucidated some of the mechanisms behind highly mobile, efficient, and robust locomotion in insects such as the cockroach. Roboticists have used this information to create biologically-inspired machines capable of running, jumping, and climbing robustly over a variety of terrains. To date, little work has been done to develop an at-scale insect-inspired robot capable of similar feats, due to limitations in fabrication, actuation, and electronics integration at small scales. This thesis addresses these challenges, focusing on the mechanical design and fabrication of a sub-2g walking robot, the Harvard Ambulatory MicroRobot (HAMR). The development of HAMR includes modeling and parameter selection for a two degree of freedom leg powertrain that enables locomotion. In addition, a design inspired by pop-up books that enables fast and repeatable assembly of the miniature walking robot is presented. Finally, a method to drive HAMR resulting in speeds up to $37 cm/s$ is presented, along with simple control schemes.

Contents

Acknowledgments

I would first like to thank my PhD advisor, mentor, and friend Professor Rob Wood. Rob is everything I could have asked for in an advisor. This work would not have been possible without the freedom, encouragement, financial and intellectual support that he has provided over the past five years.

Thank you also goes to my parents Laura and Mark. They deserve all of the credit for molding me into who I am today with their 27 years of love, guidance, and support.

I want to thank Janine for being by my side as I wrote this thesis. Her constant love, encouragement, and lunch-making were my daily sustenance throughout this tiresome writing process. Her patience with my late nights and cranky demeanor during the past several months was immeasurable, and will always be remembered.

I would like to thank Dr. Onur Ozcan, Dani Ithier, and Chris Heimlich for their contributions to the successful development of HAMR. I would also like to thank my close friends and colleagues Dr. Pratheev Sreetharan, Dr. Katie Hoffman, Dr. Yigit Menguc, Dr. Mike Tolley, and the rest of the Microrobotics Lab for all of their feedback, insightful conversations, providing an ideal work environment, and grabbing the occasional beer. I also need to thank Mike Smith and Hetchen Ehrenfeld for propping this lab on their shoulders and ensuring its continued smooth operation.

Finally, this work would not have been possible without the financial support of the US Department of Defense and Navy through the NDSEG fellowship, the Wyss Institute for Biologically-Inspired Engineering, the National Science Foundation, and the Charles Stark Draper Laboratory.

Chapter 1

Introduction and Motivations

1.1 Background

Over the past several decades, significant progress has been made to enhance terrestrial robot locomotion using principles gained from biological research. One of the key contributions from biology to legged robot designs has been the elucidation of the diverse roles of elastic elements (muscles, tendons and ligaments) in the musculoskeletal structure of running organisms in the works of Alexander [1] and Full [15]. All running animals, from insects to large mammals, utilize musculoskeletal springs distributed throughout their body to run efficiently and at high speeds. For example, the American cockroach reaches $1.5m/s$ (50 body lengths per second) [15], and cheetahs are capable of speeds up to $29m/s$ [23]. Additionally, animals such as the cockroach display amazing maneuverability [24], rapid stable gaits over rough terrain [14], [42], and the ability to climb vertical and inverted surfaces [16].

By studying high performance running animals such as the cockroach, biologists

have developed mathematical models for legged locomotion [13] and design principles that assist in the development of legged robots. Roboticists in turn have contributed to the field with physical robot instantiations that validate biologically-inspired design rules. Some key contributions include the high-performance dynamic legged robots of Raibert [38], Koditschek [40], Cutkosky [27], and Fearing [8], [22]. This is not an exhaustive list, and a good review of biologically-inspired legged robots is [54]. Through the development of biologically-inspired legged robots, these works have accomplished incredible tasks such as high speed locomotion [17], [8], [10], [40], [11], climbing vertical surfaces [34], [41], [28], [7], [6], running over rough terrain [40], [31], [30], [20], and high speed maneuverability [37].

Insect-scale mobile robots have been envisioned for exploration of a variety of hazardous environments, including collapsed buildings or natural disaster sites. A swarm of small-scale robots with embedded sensors would have the capability to access confined spaces and quickly search large areas to assist rescue efforts by locating survivors or detecting hazards such as chemical toxicity and temperature. Benefits of small scale-robots include reaching confined spaces, low cost, robustness, and favorable scaling with regards to climbing [45].

Much of the work discussed above focuses on larger scale machines, $10g$ and above, and little progress has been made in the development of at-scale insect-inspired running robots. RoaCH, a $2.4g$ hexapod was developed [22], and at the time held the title of smallest and lightest autonomous hexapod. However, RoACH's continued development occurred at a larger scale ($10g$ and above). Additionally, a centipede-inspired millirobot in the Harvard Microrobotics Lab has demonstrated remarkable capabil-

ities such as obstacle traversal and robustness to missing limbs, and has elucidated some of the mechanisms behind locomotion in many-legged animals [20].

At the millimeter and milligram scale, silicon-based walking robots have been fabricated using MEMS processes [21], [12]. Systems at this scale have demonstrated potential benefits such as large relative payload and use of batch fabrication. However, onboard power and effective ambulation have not been achieved in a MEMS-scale device.

The focus of the work on ambulatory microrobots in the Harvard MicroRobotics lab is to develop a swarm of sub-2g insect-inspired running robots capable of traversing any terrain. Numerous engineering challenges exist to reach this goal, beginning with the design and manufacturing of a single running platform; traditional macro-scale components are too large, MEMS processes are too small, and off the shelf electronics solutions do not exist. Consequently, innovation is necessary in all aspects of robot development including mechanism design, fabrication, actuation, control, and electronics.

The focus of this thesis is the mechanical design of the Harvard Ambulatory Micro-Robot, examples of which are shown in Figure 1.1. HAMR is a sub-2g legged robot manufactured using the Printed Circuit MEMS (PC-MEMS) fabrication paradigm [47] for micron to centimeter-scale systems. Highlights of the numerous HAMR prototypes include the world's smallest and lightest autonomous hexapod, locomotion speeds up to $36.9 cm/s$, and a design inspired by pop-up books that trivializes assembly and should enable future mass production.

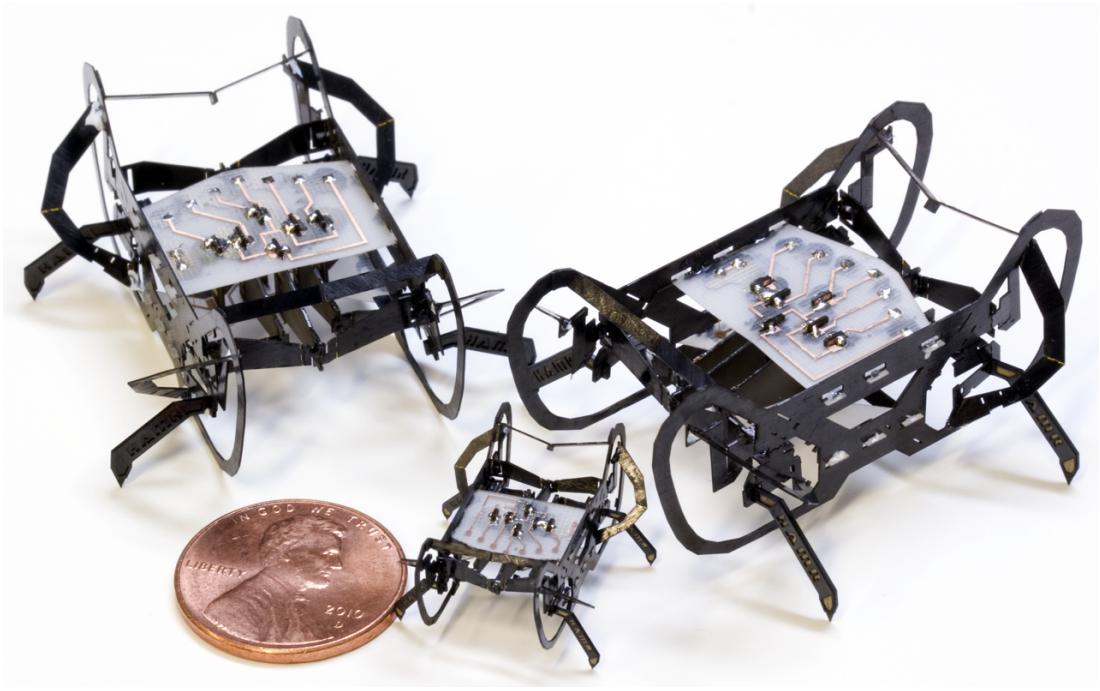

Figure 1.1: The Harvard Ambulatory MicroRobot.

1.2 Thesis Statement and Contribution

This dissertation focuses on the mechanical design, parameter selection, fabrication, and locomotion studies of the Harvard Ambulatory MicroRobot (HAMR). HAMR is a sub-2g robotic platform capable of locomotion speeds comparable to larger robots due to an intelligent design and high-performance electromechanical components. HAMR presently holds the title of the world's smallest and lightest autonomous hexapod.

1.3 Thesis Outline

This the rest of this chapter highlights prior work that enabled the development of HAMR. The additional chapters in this thesis are broken down as follows:

- Chapter 2 presents the design evolution of four Harvard Ambulatory Micro-Robot hexapods, and their contributions to the final HAMR design.

- Chapter 3 presents the design of the 2 DOF powertrain used to drive each of HAMR's legs, and theoretical and physical models used to select its parameters. In addition, an overview of the PC-MEMS manufacturing process used to fabricate HAMR prototypes is presented.

- Chapter 4 presents the design and manufacturing of the Harvard Ambulatory MicroRobot V Pop-up (HAMR-VP), the capstone of this thesis.

- Chapter 5 presents locomotion studies and a methodology to use high gait frequencies to run HAMR-VP at high speeds. In addition, a system identification of the HAMR-VP powertrain, feet that enhance friction, and maneuverability control experiments are presented.

1.4 Conventions from Biology

Throughout this work, the following terms are used, consistent with biological conventions:

- **Sagittal plane** refers to the plane bisecting a body in the vertical direction, dividing it into left and right halves. The sagittal midplane refers to the sagittal plane that generates symmetric left and right halves.

- **Transverse plane** refers to a plane that divides the body into upper and lower parts. It is perpendicular to the sagittal plane, and parallel to the ground during

flat-plane locomotion.

- **Swing phase** of a leg refers to the portion of a stride during which that leg is raised off of the walking surface, not contributing to forward locomotion.

- **Stance phase** of a leg refers to part of a stride during which that leg is on the ground, propelling the body forward during locomotion.

- **Quasi-static** refers to locomotion characterized by individual steps to move the robot forward. Quasi-static locomotion can be described kinematically, and speed is bounded by the product of stride length and frequency. The converse to this is **dynamic locomotion**, during which a body is exchanging kinetic and potential energy with compliant mechanisms in the body or leg. Speeds are theoretically unconstrained during dynamic locomotion.

1.5 Prior Work

The Harvard Ambulatory MicroRobot is an original walking robot design, however much of its manufacturing and component designs evolved from prior work. Work on the Micromechanical Flying Insect (MFI) at U.C. Berkeley [53] and later Harvard Microrobotic Fly [49], led to many technologies vital to HAMR and microrobotics in general. This work included development of a laminate manufacturing methodology for instantiation of micron- to centimeter-scale mechanical linkages relying on high efficiency flexure joints [50], [4]. The Smart Composite Microstructure (SCM) fabrication paradigm, as it was called, was used exclusively to fabricate early HAMR prototypes. SCM was also the predecessor to PC-MEMS manufacturing [47], [43],

now used to fabricate high yield and accuracy miniature mechanisms including modern HAMR designs, RoboBee [32], and a centipede-inspired walking robot [20]. In addition, work on the MFI led to the development of notional designs and models for high energy density and high bandwidth actuators suitable for microrobot locomotion using piezoelectric materials [51], [9]. The piezoelectric bending actuators that originated at U.C. Berkeley were adopted in the HAMR designs, enabling its high speed and agility.

1.6 A note on the structure of this thesis

The content of this thesis is partially drawn from the following publications:

- Chapter 2: *Design and Fabrication of the Harvard Ambulatory Micro-Robot*, A.T. Baisch and R.J. Wood. in 14th International Symposium on Robotics Research (ISRR), 2009

  Biologically-Inspired Locomotion of a 2g Hexapod Robot, A.T. Baisch, P.S. Sreetharan, and R.J. Wood. in IEEE/RSJ International Conference on Intelligent Robots and Systems (IROS), 2010.

  HAMR3: An Autonomous 1.7g Ambulatory Robot, A.T. Baisch, C. Heimlich, M. Karpelson, and R.J. Wood. in IEEE/RSJ International Conference on Intelligent Robots and Systems (IROS), 2011.

Chapter 2

Hexapedal Microrobot Designs

2.1 Introduction

One of the key contributions of this thesis is the design of a high-performance quadrupedal microrobot, the Harvard Ambulatory MicroRobot-V Pop-up (HAMR-VP) presented in Chapter 4. This chapter presents the design evolution of hexapedal HAMR prototypes that preceded HAMR-VP. The work presented here details four early robot prototypes and their contributions to the development of HAMR-VP and microrobots in general, highlighted by HAMR3: the world's smallest and lightest autonomous hexapod.

2.2 The HAMR1 Prototype

The first Harvard Ambulatory MicroRobot prototype (HAMR1) was a 90mg hexapod with overall footprint dimensions of 17 mm long x 23 mm wide (See Figure 2.1a).

HAMR1 was the first walking robot instantiated in the Harvard Microrobotics Lab using the legacy SCM fabrication paradigm [50]. The robot demonstrated the feasibility of manufacturing an at-scale insect-inspired walking robot capable of locomotion; a foundational step towards the design of HAMR-VP.

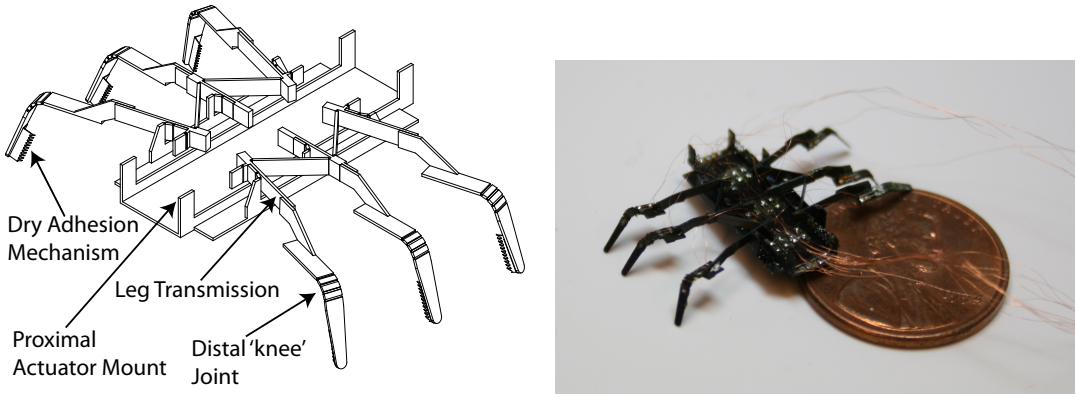

Figure 2.1: The first generation Harvard Ambulatory MicroRobot (HAMR1) made using the Smart Composite Microstructure (SCM) fabrication precess, the predecessor to PC-MEMS. Mechanical components include eight degrees of freedom (two transverse and six sagittal) driven by custom shape memory alloy (SMA) planar springs.

HAMR1's kinematic design focused on enabling the insect-inspired alternating tripod gait. Nominally, two degrees of freedom are required per leg to generate appropriate foot trajectories for locomotion; twelve total for a hexapedal robot. In HAMR1, mechanical coupling reduced the nominal 12 DOFs to an 8 DOF mechanism. Two proximal DOFs drove legs in the walking plane, each consisting of three coupled ipsilateral (same side of the body) legs; the front and rear legs swung forward and the middle leg swung rearward simultaneously, and vice-versa. Six distal knee joints raised and lowered each leg in the robot's sagittal plane. All eight DOFs were actuated using foil Nitinol shape memory alloy (SMA) springs [35], patterned using a laser

micromachining system. SMA was initially chosen due to its simple manufacturing process and input (Joule heating by a switched current source), and high strain that obviates the need for a mechanical transmission.

Each walking plane DOF was driven using antagonistic actuators rather than relying on cooling to generate bidirectional actuation. Knee joints were actuated by a single planar SMA spring coupled with a passive stainless steel spring antagonist. Actuators were heated above their transition temperature by supplying current from an off-board source through onboard circuit traces.

The robot was assembled from nine SCM components: a thorax, six legs, and two walking-plane transmissions. Circuit traces were manually aligned and epoxied to SCM components prior to final robot assembly. Actuators and antagonist springs were then soldered to bond pads provided by onboard traces. The completed HAMR1 prototype was capable of generating leg kinematics appropriate to the alternating tripod gait.

HAMR1 was capable of forward locomotion using the alternating tripod gait, albeit at slower than $1mm/s$ (0.06 body lengths per second). Actuators were powered using a constant current supply and manual push-button control, which limited gait frequency to 1Hz. A programmable controller implemented on a single leg demonstrated actuation cycles no faster than $3Hz$ due to thermal time constants of heating and cooling SMA across its transition temperature; faster actuation frequencies significantly attenuated output amplitude. At $3Hz$, each SMA spring required $274mW$ to actuate as quickly as possible without melting the solder affixing it to HAMR1's transmissions. SMA spring modeling and optimization, plus an intelligent controller

such as the one used in RoACH [22] could have improved bandwidth and power. However, all following HAMR designs instead use a different actuator technology.

2.3 The HAMR2 Prototype

The slow locomotion ($< 1mm/s$) in HAMR1 motivated improvements that led to the design and instantiation of the HAMR2 prototype (See Figure 2.2). HAMR2 was a $5.7cm$ long and $2g$ hexapod (scaled up from HAMR1 due to the difficulties of manual assembly) capable of tethered locomotion up to $22.8cm/s$, a significant improvement over HAMR1. The HAMR2 design introduced two key features used in HAMR-VP that improve locomotion speed: piezoelectric actuation and the two DOF spherical hip joint, detailed in Chapter 3.

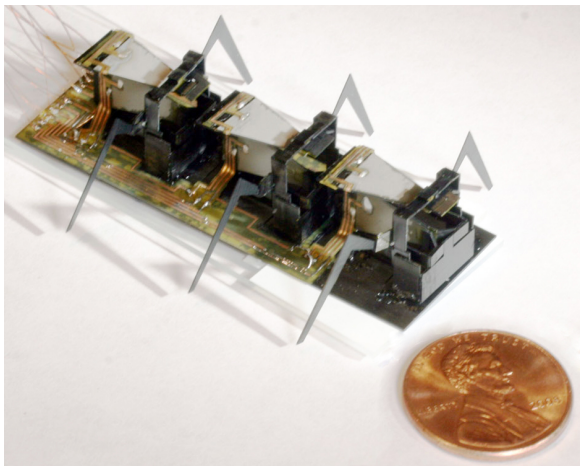

Figure 2.2: The second generation Harvard Ambulatory MicroRobot (HAMR2).

2.4 HAMR3, The World's Smallest and Lightest Autonomous Hexapod

The third generation Harvard Ambulatory MicroRobot (HAMR3) is a $1.7g$, $4.7cm$ long autonomous hexapod robot (see Figure 2.3). At the time of its inception, HAMR3 was the smallest and lightest hexapod capable of autonomous locomotion. HAMR3's mechanical design was similar to HAMR2, however its body was made from a custom printed circuit board to house onboard electronics. Additionally, the development of HAMR3 led to an improved piezoelectric actuator with embedded circuit traces (see Chapter 3).

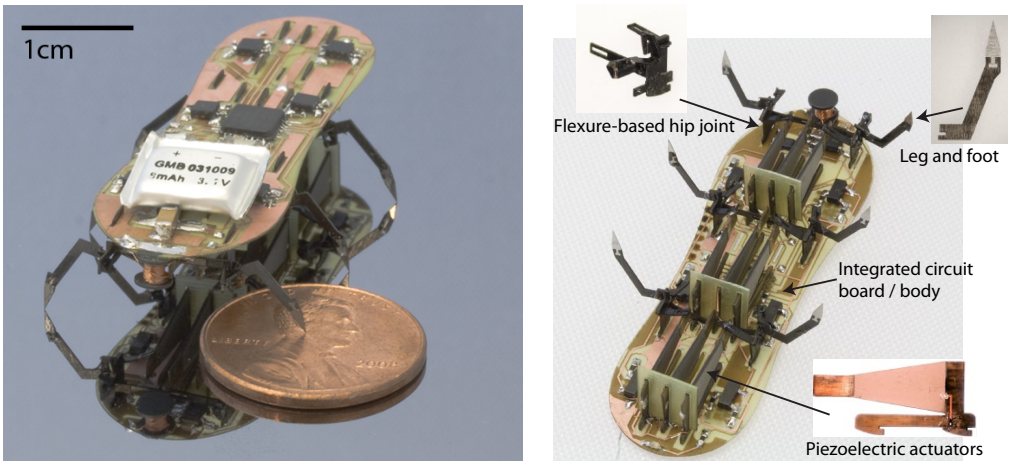

Figure 2.3: The third generation Harvard Ambulatory MicroRobot (HAMR3). Shown here is the completed robot with on-board electronics and battery (left) and an illustration of the robot mechanical design (right).

The walking performance of tethered HAMR prototypes suffer from the use of external electronics. The experimental setup used for power and control consists an xPC target environment (requiring two PCs) for control and high-voltage signal generators for power (see Figure 2.4). In order to achieve autonomy, onboard electronics

must provide the following functions for a robot in a package that fits on the $1g$, $4.7cm$ mechanical structure: power conditioning, boost conversion, gait timing, and sensor processing. Off-the-shelf solutions do not exist to convert typical battery outputs $(3.7 - 5V)$ to piezoelectric actuator input voltages $(200 - 300V)$ at HAMR's scale, and therefore a custom circuit design was required.

A solution was developed by visiting graduate student Christian Heimlich that is detailed in [19], [5]. The design implemented an autotransformer boost converter topology [26] and a microcontroller for feed-forward gait generation. HAMR3 was capable of untethered flat ground locomotion for up to $4.3cm/s$ using $200V$ drive inputs and a $20Hz$ gait frequency. Using an $8mAHr$ lithium polymer battery, the robot could sustain locomotion for up to 2.5 minutes per charge.

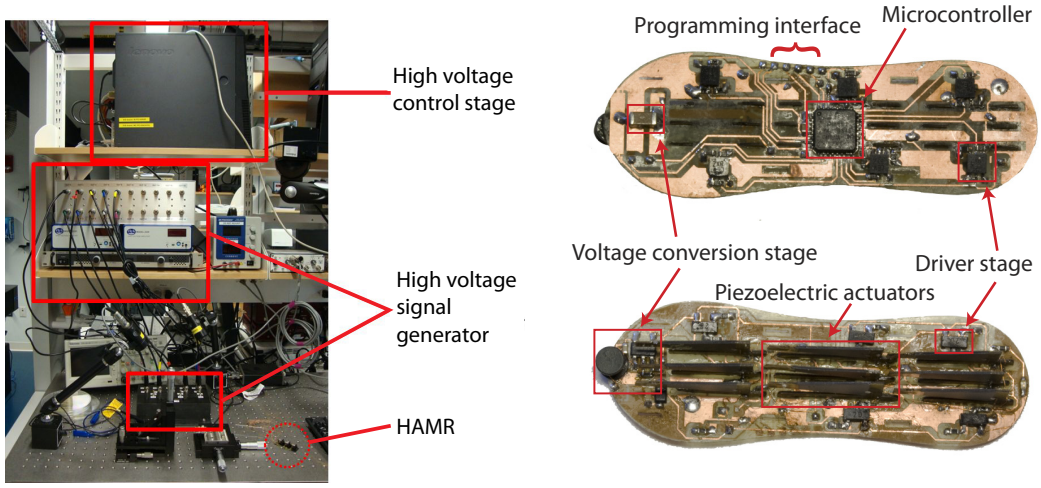

Figure 2.4: The off-board circuitry used for power and control of tethered HAMR prototypes, with the HAMR2 robot for scale (left). HAMR3's onboard electronics replicate the functionality of off-board circuitry in an $800mg$ package.

Due to the additional mass from onboard electronics, HAMR3's powertrain could not sufficiently supporting itself. The result was locomotion characteristic of stick-

slip behavior; swing phase legs did not leave the ground, however reduced friction to allow stance legs to drive the robot forward. This behavior precluded locomotion over anything but perfectly flat terrain, and motivated powertrain studies in Chapter 3.

2.5 The HAMR4 Prototype

The HAMR4 prototype was a demonstration of the diverse materials usable in a PC-MEMS laminated structure. Its rigid exoskeleton was made from 4-ply $[0, 90]_s$ carbon fiber, a Kapton flexure, and copper-clad FR4 circuit board. Additionally, the multi-layer circuit exoskeleton design used in HAMR-VP was introduced in HAMR4. Unfortunately, HAMR4 was too heavy for its powertrain to support; its body would sag to the ground, preventing forward locomotion. This result further motivated the powertrain studies to improve payload in Chapter 3.

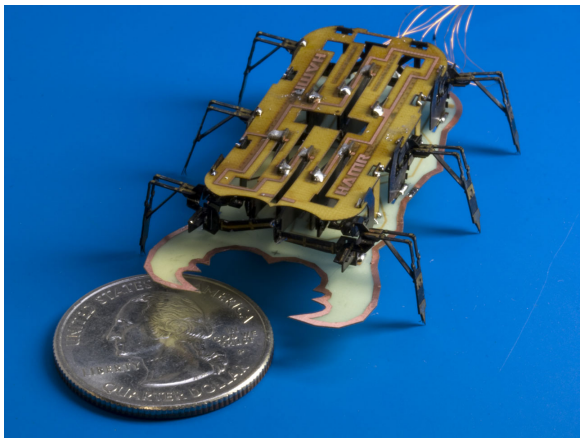

Figure 2.5: The fourth generation Harvard Ambulatory MicroRobot (HAMR4).

2.6 Discussion

Four robot prototypes were presented here that preceded the HAMR-V and HAMR-VP designs in Chapter 4. A summary of their performance is in Table 2.6, which will be re-visited in Chapter 6 to compare HAMR-VP to its predecessors. Several key contributions were made through the development of these hexapedal HAMR designs that persisted in HAMR-VP. The most notable include the selection and design of high-bandwidth piezoelectric actuators (HAMR2-HAMR4), the design of a two-DOF spherical hip joint (HAMR2), and onboard electronics that enable autonomy (HAMR3).

Table 2.1: Summarizing HAMR Prototype Results

Robot	**Mass** (g)	**Length** (cm)	**Gait Frequency** (Hz)	**Speed** (cm/s)	**Normalized Speed** (body lengths s^{-1})
HAMR1	0.09	1.7	1	< 0.1	< 0.1
HAMR2	2	5.7	20	23	4
HAMR3	1.7	4.7	20	4.3	0.9
HAMR4	2	5.3	1	0	0

Chapter 3

Powertrain Design, Manufacturing, and Parameter Selection

3.1 Introduction

This chapter details the two degree of freedom (DOF) powertrain design (actuators and transmissions) used to drive each leg in the Harvard Ambulatory MicroRobots. Each element of the powertrain will be presented, including the piezoelectric bending actuators, flexure-based four-bar transmissions, and spherical five-bar hip joint. Furthermore, mathematical and physical models of the HAMR powertrain will be discussed and used to select parameters for the HAMR-V and HAMR-VP designs in Chapter 4. In addition, an overview of the PC-MEMS manufacturing process used to manufacture the mechanical components of each HAMR prototype will be presented here.

3.2 Microrobot Manufacturing

HAMR's mechanical components were manufactured using the Printed Circuit Microelectromechanical Systems (PC-MEMS) fabrication paradigm [47]. The process was named for its use to fabricate micron to centimeter-scale systems using techniques adopted from layered printed circuit manufacturing. PC-MEMS manufacturing was primarily developed by Dr. Pratheev Sreetharan and Dr. Peter Whitney in the Harvard Microrobotics Lab, and is the successor to the Smart Composite Microstructure fabrication paradigm introduced by Professor Rob Wood *et al.* at the University of California, Berkeley [50]. This paradigm has enabled the creation of numerous milli- and micro-robots including HAMR, a centipede-inspired millirobot [20], and the Harvard RoboBee [48].

To illustrate PC-MEMS manufacturing, a case study of the spherical five-bar hip joint used in HAMR3, HAMR4, and HAMR-V is presented in Figure 3.1. While a diverse set of materials and arbitrary layer count can be used with the PC-MEMS manufacturing process, the design presented here consists of a five layer standard linkage laminate (SLL): a Kapton flexure at the laminate mid-plane, two rigid carbon fiber exterior layers, and two sheets of acrylic adhesive to bond subsequent layers. Each layer is first patterned using a $355nm$ UV diode-pumped solid state (DPSS) laser. This first laser machining step includes cutting flexure gaps into carbon fiber and adhesive layers, and alignment features in all layers. The five layers are stacked on an assembly jig using dowel pins for alignment, followed by lamination under heat and pressure. The laminate is realigned under the DPSS laser, and final cuts are made to release the structure. The resulting parts can then be assembled by folding

into an articulated 3D mechanism. Manufacturing tolerances using the PC-MEMS process are $1 - 10\mu m$ based on laser beam diameter and pin alignment. Assembly tolerances are design-dependent, and will be discussed in Chapter 4.

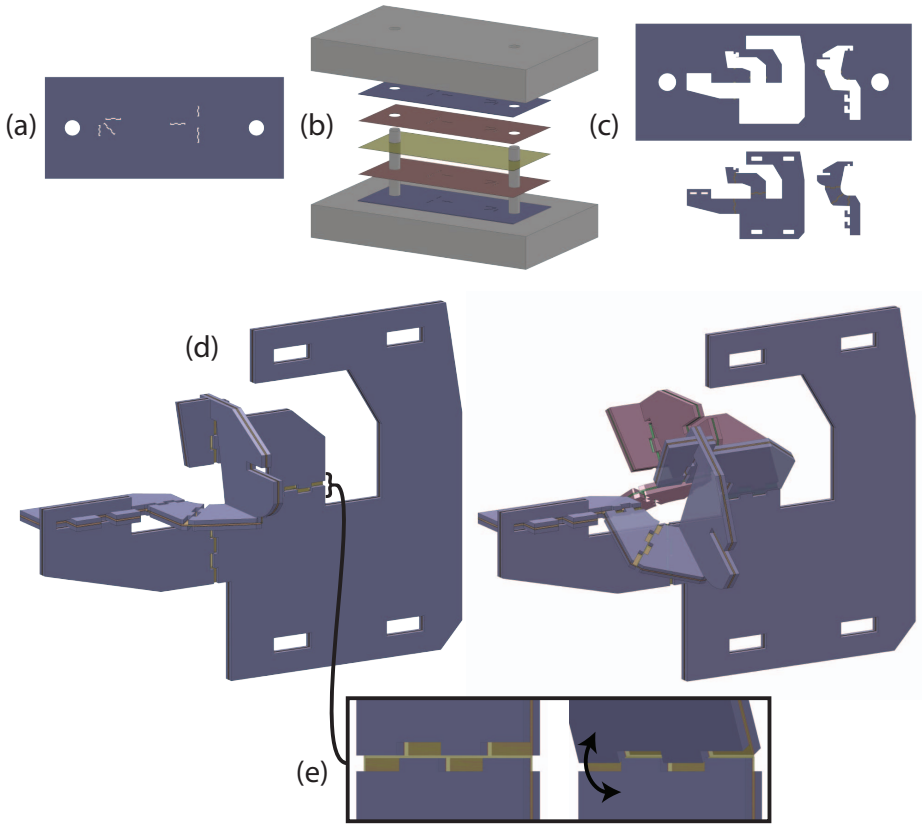

Figure 3.1: The Printed Circuit Microelectromechanical Systems (PC-MEMS) manufacturing paradigm invented in the Harvard Microrobotics Lab by Dr. Pratheev Sreetharan and Dr. Peter Whitney. Fabrication of a HAMR spherical five-bar hip joint is depicted here. Using a UV diode-pumped solid state (DPSS) laser, flexure gaps and assembly features are machined into each layer (a). Layers are stacked using dowel pins for alignment (b), then cured under heat and pressure. The resulting laminate is laser-machined to release the final parts (c), which assemble into an articulated 3D structure (d). Flexure joints use a casselated design to prevent collisions between carbon fiber links (e).

An important component of the mechanisms in HAMR is the casselated flexure joint developed by Sreetharan (see Figure 3.1e). Casselations prevent link collisions

in joints with flexure length smaller than carbon fiber link thickness. This allows near-ideal pin joint behavior and prevents flexure buckling. The tradeoff is higher joint stresses, and thus shorter lifetime (fewer cycles to failure), however casselated flexures in HAMR prototypes have lasted greater than 10^5 cycles before failure.

Printed Circuit Board Manufacturing Single or double-sided printed circuit boards for HAMR are fabricated in the Harvard MicroRobotics Lab using a custom in-house manufacturing method. Clean, un-patterned boards ($127\mu m$ copper-clad FR4) are first spin-coated with a thin layer of photoresist and baked to remove solvents. Photoresist is selectively removed by ablation using the $355nm$ UV DPSS laser at a low power, preventing damage to the underlying copper. The circuit is placed in a wet chemical etchant (Ferric Chloride) to remove exposed copper. The resulting printed circuit boards (see Figure 3.2) were used to trace off-board power and control signals to their respective actuator or support on-board electronics (in HAMR3).

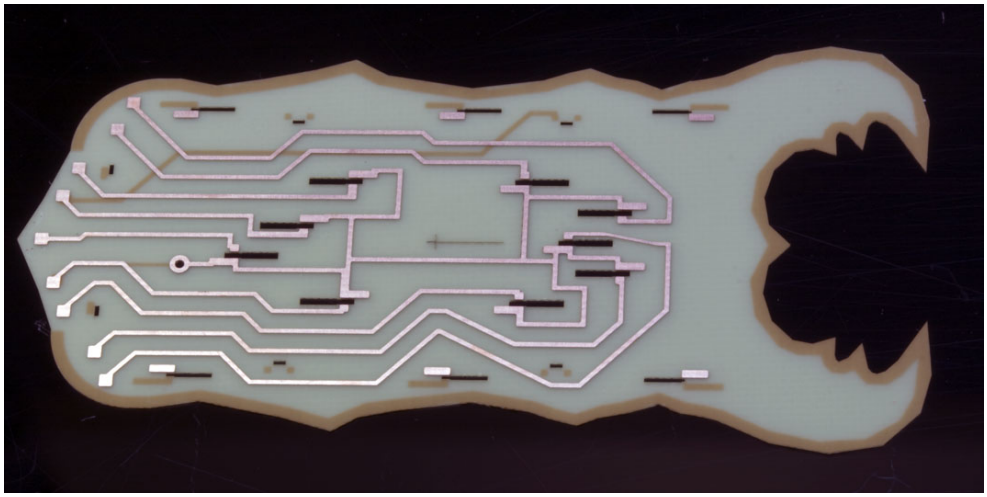

Figure 3.2: Single or double-sided circuit boards are fabricated with a custom in-house manufacturing process. The HAMR4 double-sided insect-inspired body is shown here.

3.3 Spherical Five-Bar Hip Joint Design

For quasi-static operation, legged robots require two-dimensional foot trajectories in the sagittal plane for successful locomotion, i.e. each foot requires a quasi-elliptical path in the vertical plane to take a step. This requirement is trivial in larger legged or 'whegged' robots that use continuously rotating actuators (e.g. DC motors) and mechanical components (e.g. gears and pin joints) to generate foot trajectories with a single degree of freedom [40], [2], [8], [17]. Constrained by linear actuators and flexure joints inherent to the PC-MEMS process, HAMR requires two degrees of freedom per leg to generate similar trajectories.

One solution for a 2 DOF flexure mechanism is a serial kinematic chain with actuators mounted at each joint, such as HAMR1's proximal drive and distal control actuators. However, the ideal leg mechanism minimizes actuation complexity while concentrating mass proximal to the body. To achieve this design goal, a new spherical five-bar (SFB) linkage was created by Dr. Pratheev Sreetharan. The SFB maps two decoupled drive inputs to a 2 DOF output leg motion (see Figure 3.3a) at a near 1-to-1 transmission ratio. The SFB is a parallel mechanism with both input links executing simple rotations with respect to the linkage ground. Since all actuation is referenced to the robotic body, actuator mass can be proximally concentrated.

From the neutral configuration, actuation of the drive DOF input causes a rotation of the output leg about an axis perpendicular to the walking plane through the SFB spherical center. Independent of leg drive angle, actuation of the lift input causes an output leg rotation about an axis in the walking plane perpendicular to the leg and through the SFB spherical center. A kinematic analysis performed by Dr. Sreetharan

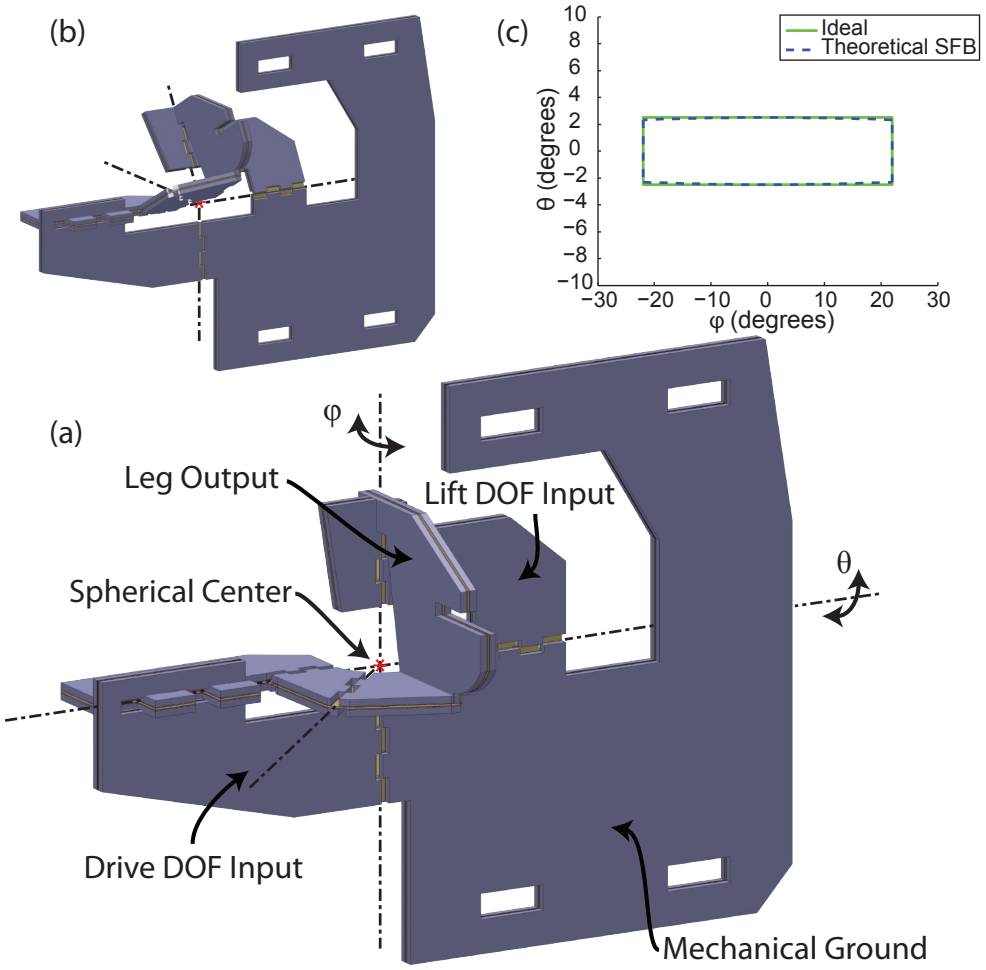

Figure 3.3: The spherical five-bar (SFB) hip joint used in HAMR, designed by Dr. Pratheev Sreetharan (a). The SFB enables proximal actuation of two parallel degrees of freedom acting on a single end effector. In HAMR, these DOFs correspond to a 'lift' that raises and lowers the leg in the sagittal plane (b), and an orthogonal 'drive' that provides locomotive power in the walking plane. A kinematic analysis courtesy of Dr. Sreetharan shows that in theory the two DOFs are largely decoupled (c).

of the 2 DOF spherical five-bar shows that outputs are largely decoupled, providing independent control of lift and drive angles (see Figure 3.3c). The decoupled leg motion results in a simple mapping between actuation inputs and leg orientation, simplifying powertrain modeling and control system design in HAMR.

3.4 Piezoelectric Actuator Design and Manufacturing

HAMR's legs are driven using optimal energy density piezoelectric bending bimorph actuators [51] (see Figure 3.4). At HAMR's scale, piezoelectric actuators are advantageous for their efficiency, energy density, and bandwidth over an alternative such as shape memory alloy (see the HAMR1 prototype in Chapter 2). Furthermore, a design and manufacturing solution for piezoelectric actuators in microrobots existed in the Harvard Microrobotics Lab prior to the development of HAMR, thus additional development of actuator solutions was unnecessary. As mentioned in Chapter 1, the notional design, mathematical model, and manufacturing process for an optimal energy density (actuator energy output divided by mass) actuators were developed by Professor Rob Wood for the Harvard Microrobotic Fly.

The actuators in HAMR are bending clamped-free cantilever beams, meaning they are mechanically grounded at their base and generate a bending motion at their tip. Output displacements are small ($50 - 200\mu m$), and thus require a transmission for amplification to appropriate leg displacements for locomotion. The actuators are voltage driven using a simultaneous drive method [25], whereby a constant high voltage bias is supplied across outer actuator plates and a drive signal to the central electrode. Typical bias and drive voltages range from 100V-300V, posing a difficult challenge in the implementation of onboard electronics in microrobots. A solution was developed for HAMR3 to enable autonomy (see Chapter 2), however the primary focus of this work was on HAMR's mechanical design and manufacturing and therefore all

other prototypes use external power and control to shorten the design and prototyping cycle.

The actuator manufacturing process evolved with efforts by myself and other Microrobotics Lab members to improve yield and repeatability, and enable parallel fabrication; requirements for robots with multiple actuators such as HAMR. HAMR's actuators are manufactured as a three-plane laminate using three constituent materials: 1) two $127\mu m$ lead zirconate titanate (PZT) piezoelectric ceramic plates (PZT-5H, Piezo Systems), 2) a central carbon fiber layer (M55J fibers, RS3C resin), and 3) custom printed circuit boards (copper-clad FR4). The bottom and top layers of an actuator each consist of a PZT plate bounded in-plane at the base and tip by copper-clad FR4. At the base, copper traces connect three actuator inputs to the two outer PZT plates (bias and ground) and the central electrode (drive signal). FR4 at the actuator tip electrically insulates the PZT plates and central electrode from attached carbon fiber transmissions. Furthermore, FR4 serves to align and constrain actuator plates during manufacturing. The central layer of each actuator consists of a 1 to 3-ply sheet of unidirectional carbon fiber, which begins the manufacturing cycle as an uncured prepreg. The layers are laminated under heat and pressure, using resin from the prepreg carbon fiber as an adhesive. A set of actuators are manufactured in parallel using the method illustrated in Figure 3.4.

3.5 A HAMR Powertrain Model

The HAMR powertrain consists of a single 2 DOF spherical five-bar hip joint, defining the lift and drive DOFs of a single leg. Each input to the SFB is driven by

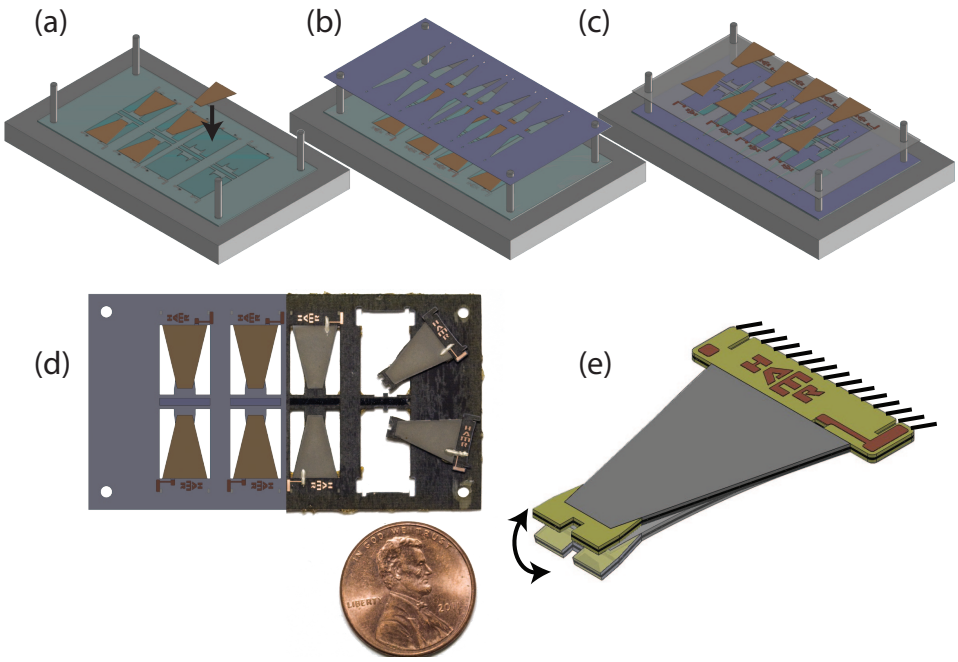

Figure 3.4: HAMR uses optimal energy density piezoelectric bending bimorphs [51] to actuate its 2 DOF powertrain. Actuator fabrication uses similar process steps to PC-MEMS manufacturing. First, two printed circuit boards ($127\mu m$ copper-clad FR4) are custom-patterned using the process described in Section 3.2. Bulk $127\mu m$ PZT-5H is scored using a $355nm$ UV laser and cleaved to produce two trapezoidal plates per actuator. The first actuator layer is assembled using pick and place methods to align PZT plates in-plane with an FR4 layer (a). Individual plates are constrained during the layup process by a tacky substrate (Gelpak) and spring clips built into the FR4 structure. A 1 to 3-ply central carbon fiber layer (M55J fibers, RS3C resin) is laser-cut and aligned with the bottom active layer using dowel pins (b). The top FR4 and PZT layer is assembled similarly to (a) and stacked to complete the actuator laminate (c). The carbon fiber resin is cured under heat and pressure, laminating the three layer structure. Finally, conductive epoxy is applied to each actuator to connect PZT plates and copper traces, followed by a final laser-cut release of HAMR's actuators (d). The resulting actuator produces a bending motion in response to applied voltage across each piezoelectric plate, which drives 1 DOF of HAMR's powertrain.

a piezoelectric bending actuator, with displacement amplified by a four-bar flexure-based transmission. Using the assumption that SFB outputs are largely decoupled, the HAMR powertrain can be modeled as two single DOF systems, each consisting

of an actuator, four-bar transmission, and leg (see Figure 3.5).

Actuators are modeled as a force source, F_{act} in parallel with a linear spring with stiffness k_{act} and tip displacement δ_{act}. Actuator resonance is assumed on the order of 1KHz, well above the stride frequencies (1-70Hz) used in HAMR. The actuator is therefore operating quasi-statically and its mass is ignored. A serial compliance, k_{ser} is included between the actuator output and transmission input to represent compliance observed in the robot due to a non-rigid exoskeleton and off-axis flexure bending (buckling and twisting). The four-bar transmission takes an input displacement δ_{tra} and has rigid, approximately massless links with lengths $L_{(j=1,2,3)}$. Flexures in the four-bar transmission are modeled as ideal pin joints with angular displacement ϕ_i and a linear torsional spring with stiffness κ_i $(i = 1, 2, 3)$. A pin joint approximation is satisfied by the casselated flexure design described in Section 3.2. Legs are modeled as a rigid, massless extension from the four-bar transmission output with horizontal and vertical dimensions L_{Leg-x} and L_{Leg-y}, respectively. The entire system model is lossless; a system ID in Chapter 5 confirms that the powertrain behaves like an under-damped 2nd-order system with damping ratio between $0.06 - 0.12$. Powertrain parameter selection will be discussed in Section 3.6.

A transmission 'bias' not shown in the model can be introduced by changing the length of the input link between actuator and transmission. Changing the input link length without modifying the actuator and transmission ground locations requires pre-straining the transmission to attach it to the actuator. As a result, the transmission ratio around the neutral leg position varies with the changing moment arm caused by rotation of the leg. Furthermore, input link bias preloads the transmission flexures,

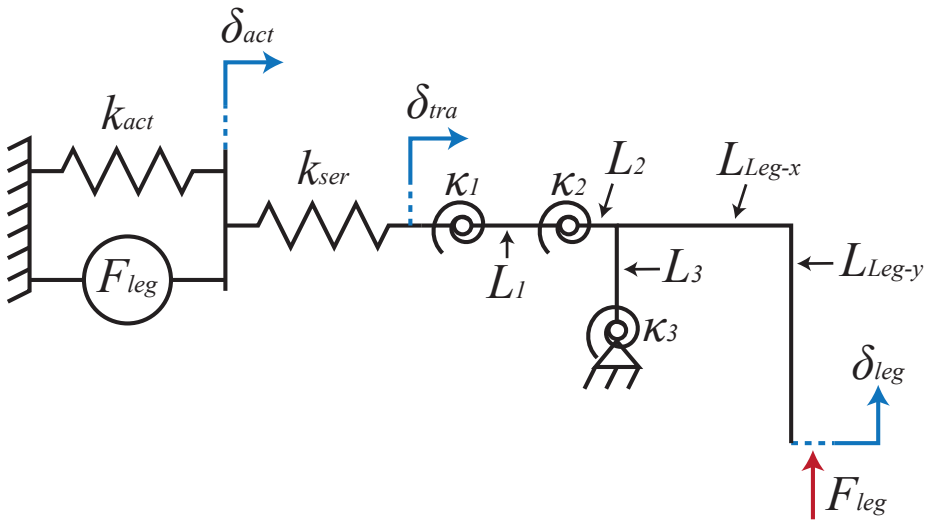

Figure 3.5: Single degree of freedom model of the HAMR lift DOF powertrain. An actuator, modeled as a force source in parallel with compliance k_{act}, drives a four-bar flexure-based transmission with torsional stiffness κ_i and link lengths L_j to impart a blocked force or displacement at the tip of a leg. A serial spring stiffness k_{ser} represents non-ideal characteristics of the robot such as exoskeleton and flexure off-axis compliance (twisting and buckling).

thus increasing resistance to the robot mass.

3.5.1 Kinematics and Dynamics

Kinematics of the HAMR powertrain are analogous to a four-bar slider-crank mechanism. A known solution exists for slider-crank kinematics in [46]. The loop-closure equations for the HAMR transmission were solved and the results map transmission input displacement, δ_{tra} to three four-bar joint angles, ϕ_1, ϕ_2, ϕ_3 and vertical plane leg displacement δ_{leg}.

A balance of power terms in the model in Figure 3.5 maps actuator force/displacement to leg force/displacement and can be used to solve for loading scenarios during quasi-static locomotion. A full derivation is in Appendix A and the final equation used to

map input to output is given by:

$$AF_{\text{act}} - Ak_{\text{act}}\delta_{\text{tra}} + \kappa_1\Phi_1\frac{\partial\Phi_1}{\partial\delta_{\text{tra}}} + \kappa_2\phi_2\frac{\partial\Phi_2}{\partial\delta_{\text{tra}}}\ldots + \kappa_3\Phi_3\frac{\partial\Phi_3}{\partial\delta_{\text{tra}}} - F_{\text{leg}}R_{\text{tra}} = 0, \quad (3.1)$$

where $R_{\text{tra}} = \partial\delta_{\text{leg}}/\partial\delta_{\text{tra}}$ is the relative movement of the leg with respect to the movement of the transmission input; hence it is the instantaneous transmission ratio. The terms $\frac{\partial\Phi_1}{\partial\delta_{\text{tra}}}$, $\frac{\partial\Phi_2}{\partial\delta_{\text{tra}}}$, $\frac{\partial\Phi_3}{\partial\delta_{\text{tra}}}$, R_{tra} and δ_{tra} can be solved kinematically for a given leg displacement and the force experienced by the leg can be found with known stiffness and transmission geometric parameters, and modeled or experimental actuator outputs. The full system equation is solved numerically using MATLAB's fsolve command.

3.6 Powertrain Parameter Selection

Hexapedal HAMR prototypes in Chapter 2 suffered from a powertrain incapable of supporting the robot's mass in the sagittal plane (sagging). Sagging decreased swing phase foot lift displacement enough to cause locomotion by a stick-slip mechanism rather than stepping (in HAMR2 and HAMR3). This precluded locomotion on anything but perfectly flat terrain. In an extreme case, the robot's thorax sagged to the ground, preventing forward locomotion (in HAMR4).

Improving HAMR's lift-DOF performance was approached from three directions: 1) reducing robot mass, 2) reducing powertrain serial compliance, k_{ser}, and 3) carefully selecting powertrain parameters. Here, the HAMR powertrain model and a physical

instantiation of a single leg mechanism are used to select appropriate powertrain parameters. Exoskeleton and transmission compliance are improved with the design of HAMR-VP in Chapter 4.

Three design criteria for the HAMR powertrain were developed from scenarios experienced during locomotion:

Criteria 1: When actuators are off, the robot must passively support itself by preventing sag past a critical point after which the active legs are unable to lift the robot (unlike HAMR4); $F_{act} = 0$, $F_{leg} = M_{HAMR}/N$ where M_{HAMR} is the robot mass, and N is the total number of legs ($N = 6$ for a hexapod and $N = 4$ for a quadruped).

Criteria 2: During the stance phase of locomotion, the active leg must support at least half of the robot's weight while other legs are removed from the walking surface; $F_{act} > 0$, $F_{leg} \geq M_{HAMR}/2$.

Criteria 3: During the swing phase of locomotion, a large vertical displacement, δ_{leg} is required to enable locomotion over rough terrain. A minimum of $2mm$ is desirable; $F_{act} < 0$, $F_{leg} = 0$.

In this section two approaches are taken to satisfy the above criteria: 1) increasing powertrain energy density and 2) tuning transmission parameters to find an appropriate tradeoff between output force and displacement.

3.6.1 Actuator Characterization

According to a laminate flat plate model for optimal energy density piezoelectric bimorphs in [51], actuator energy density is independent of its planar dimensions (i.e. length and nominal width). Therefore, the effect of material thicknesses on energy density was investigated. PZT is acquired from the manufacturer in discrete thicknesses down to $127\mu m$, and therefore difficult to scale; scaling up would require nearly doubling the actuator mass. The central elastic (carbon fiber) layer contributes minimally to actuator mass and is available in more discretized thicknesses than PZT. Therefore, actuators with elastic layers consisting of 1, 2, and 3 sheets ($66, 116$, and $166\mu m$ thick) of carbon fiber were manufactured and characterized.

The model in [51] suggests that there exists an optimal carbon fiber thickness for actuator energy density. The optimum value is based on a tradeoff between actuator mass and the moment arm between the actuator mid-plane and stress-inducing PZT plate. Scaling up elastic layer thickness increases both mass and the PZT-to-midplane moment arm, the latter of which has an optimum value. Figure 3.6 shows that experimentally, the highest energy density was achieved with 2-ply carbon fiber, making it the choice for HAMR's actuators.

Additionally, actuators were driven to failure by blocking the tip output and steadily increasing voltage. The HAMR 2 ply carbon fiber actuators failed at 300-350V. A maximum 250V bias and drive voltage was chosen to reduce the chance of actuator failure in HAMR.

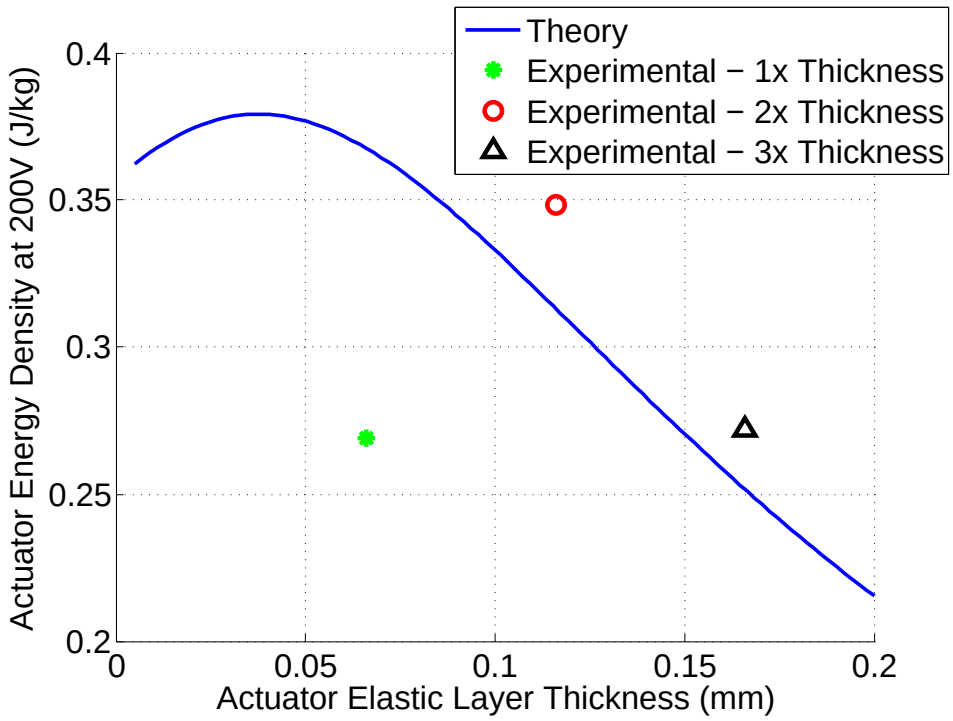

Figure 3.6: Optimizing the HAMR actuator elastic layer (carbon fiber) thickness. Three actuators each with 1, 2, and 3-ply carbon fiber were fabricated and their outputs characterized using a force sensor (Nano17, ATI Industrial Automation) for blocked force F_b and optical microscopy for displacement δ_{max}. Results are presented as energy density (mechanical energy output divided by actuator mass) for one half actuator cycle, $E = F_b\delta_{max}$. Experimental data points represent the mean results of three trials each for three actuators. The results show that at the same drive voltage, 2-ply carbon fiber has a higher energy density than 1 or 3 ply. This result was implemented into the actuator design for HAMR-V and HAMR-VP in Chapter 4.

3.6.2 Single DOF Powertrain Experiments

A physical model was developed to investigate the inadequate lift DOF performance in early HAMR prototypes (see Figure 3.7). Additionally, an experimental setup was constructed to measure up to two axes of force and displacement at the robot's foot. The single leg setup in Figure 3.7 consists of a 1 or 2 DOF HAMR powertrain and two single axis force sensors (RSP2, Loadstar Sensors) that can be

oriented to measure any combination of vertical and lateral plane forces. Only vertical plane forces were recorded for the work in this chapter, however the setup was used to characterize lateral foot-ground friction forces in Chapter 5. Additionally, a camera (PL-B741F, Pixelink) mounted perpendicular to the lift DOF plane was used to record foot displacement. A single-axis motorized stage (UTS100PP, Newport) was used to prescribe vertical displacement offsets to the single leg mechanism.

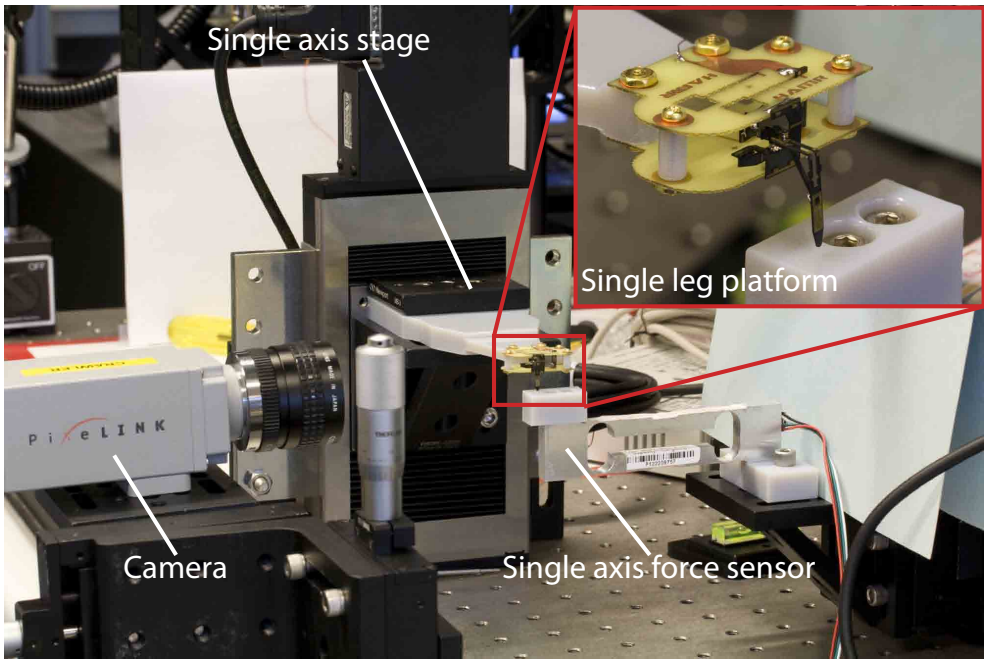

Figure 3.7: The HAMR single leg experimental setup enabled measurement of force and displacement outputs from a 1 or 2 DOF HAMR powertrain. The setup consists of two single-axis sensors (RSP2, Loadstar Sensors) to measure any combination of vertical and lateral forces (only vertical shown), a camera (PL-B741F, Pixelink) to record leg displacements, and a single-axis motorized stage (UTS100PP, Newport) to control the powertrain's vertical displacement.

To improve the HAMR transmission design from previous prototypes, two parameters with a substantial effect on performance were varied: flexure stiffness κ_i and input bias. Flexure stiffness can be affected by joint geometry or material (i.e. elastic

modulus). Kapton polyimide (Dupont) is the chosen material for microrobot flexures due to its high mechanical strength and resilience, which enable it to undergo many (greater than 10^5 in HAMR) cycles before failure. Assuming flexure joints behave like bending beams of length l, with rectangular cross section of width w and thickness t, torsional stiffness as a function of geometry behaves according to

$$\kappa_i \propto \frac{w_i t_i^3}{l_i}$$

Increasing flexure thickness has a cubic relationship with torsional stiffness and requires no design changes to the HAMR transmission, making it a good choice for an experimental tuning parameter in this study. Furthermore, l and w were constrained to ensure near-ideal pin-joint behavior, and prevent collisions with the drive DOF transmission, respectively. In addition to flexure thickness, an input link bias was implemented to affect transmission ratio and flexure preload.

Four HAMR lift DOF powertrains were fabricated with parameters summarized in Table 3.6.2. A fifth transmission was built with a 2 DOF SFB hip joint to identify coupling or off-axis compliance due to the addition of a second orthogonal (drive) DOF. Flexure thicknesses of $12.5\mu m$ and $25\mu m$ were chosen based on commercially available Kapton material. HAMR prototypes susceptible to sagging used $12.5\mu m$ thick material and is therefore considered the 'baseline' design. A $200\mu m$ input link bias was chosen for the 'Biased' design to match the average actuator deflection at 250V; the neutral leg position of a 'Biased' transmission is identical to the case $F_{act}(V) = F_{act}(250V)$ of a 'Baseline' transmission.

Experimental blocked force and free displacement data were collected using each

Table 3.1: Transmission Designs

Design	**Flexure Thickness** (μm)	**Bias Length** (μm)	**DOFs**
Baseline	12.5	0	Lift Only
2x Kapton	25	0	Lift Only
Bias	12.5	200	Lift Only
2x Kapton and Bias	25	200	Lift Only
2 DOF 2x Kapton and Bias	25	200	Lift and Drive

of the five transmissions driven by the 2-ply carbon fiber actuators described above. Blocked force data was collected for $F_{act}(250V)$ using a motorized stage to simulate sag heights from 0 to $3mm$. Free leg lift displacement was measured optically for drive voltages of 100 to 250V at 50V increments. Experimental powertrain force and displacement outputs are shown in Figure 3.8.

Passive powertrain stiffness was evaluated by prescribing known vertical displacements to the single leg system and recording ground reaction force. Data was collected starting with the leg in its neutral configuration, barely in contact with the force sensor. The system was driven down at a rate of $10\mu m/s$ to a maximum displacement of $2.5mm$, then returned to the neutral configuration at the same speed. Experimental results were susceptible to artifacts from stick-slip behavior in the lateral plane, causing a large variance between the forward and return direction force measurements. Results in Figure 3.8c are therefore simulations of the powertrain model in Section 3.5 that lie between forward and reverse stiffness measurements. Simulation parameters included measured actuator stiffness k_{act} and known linkage geometry $L_{j=1,2,3}$, L_{Leg-x}, and L_{Leg-y}. Flexure torsional stiffnesses $\kappa_{i=1,2,3}$ and serial compliance k_{ser} were fit to the powertrain model using results from the active force and displacement experiments above. Fit parameters and model simulations were contributed by Dr. Onur

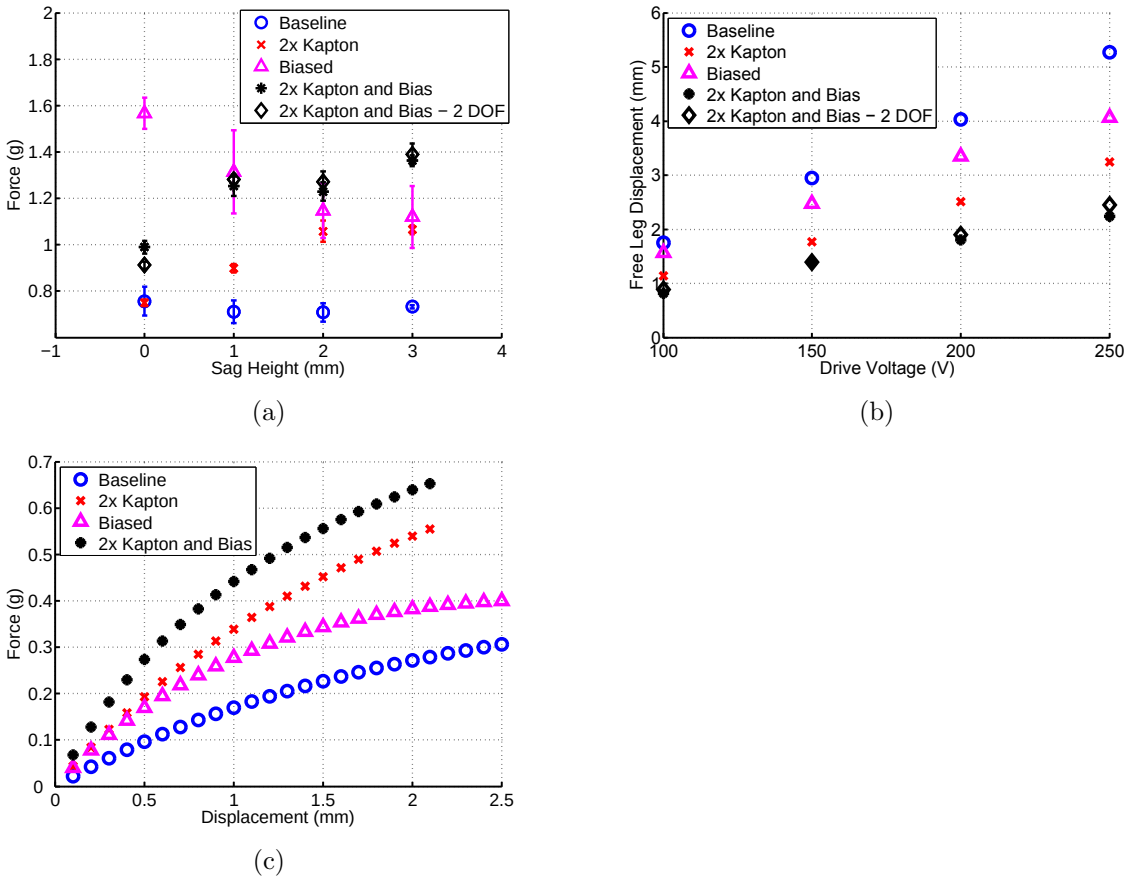

Figure 3.8: HAMR single leg experimental results. Thanks to Dani Ithier for her assistance with experimentation and Dr. Onur Ozcan for data analysis, parameter fitting, and model simulations. Measured characteristics of each HAMR powertrain were: blocked force with simulated sag at 250V drive voltage (a), free leg vertical displacement as a function of actuator voltage (b), and passive powertrain stiffness (c). Data and error bars in (a) represent the mean and standard deviation of five trials.

Ozcan.

The results of this parameter study led to the selection of a powertrain design for the HAMR-V and HAMR-VP robots in Chapter 4. Of the four experimental transmission designs, the two with biased input link designs robustly satisfy Criteria 2 for HAMR-V and HAMR-VP by actively supporting half of their weight ($5.25mN$

and $6.23mN$, respectively). The 'Baseline' transmission design marginally supports the robot weights at the neutral leg position. Furthermore, the transmission softens (i.e. output force decreases with increasing sag height) due to the increasing moment arm as a result of leg rotation. Conversely, the '2x Kapton' transmission displays a desirable stiffening (i.e. output force increases with sag height). This stiffening is due to a higher flexure stiffness that counteracts the increased moment arm as the robot sags. However, the '2x Kapton' transmission marginally satisfies Criteria 2 and is therefore not robust to additional payload.

Comparing the performance of the two biased transmissions at their neutral configuration, the 'Biased' transmission outperforms the '2x Kapton and Bias' transmission in force output by a factor of 1.6 and free displacement by a factor of 1.9 using $250V$ inputs. However, due to its stiffer flexures, the '2x Kapton and Bias' transmission is more robust to sag. Similar to the 'Baseline' transmission, the 'Biased' design experiences a softening when it is preloaded; the '2x Kapton and Bias' stiffens. The higher transmission stiffness in the '2x Kapton and Bias' design also benefits sag height under a static payload. It is possible that the $1.07g$ HAMR-V and $1.27g$ HAMR-VP would have comparable, if not more effective quasi-static locomotion performance using a 'Biased' transmission. However a large payload capacity is required for onboard electronics, which dictates the selection of the '2x Kapton and Bias' design. In the future, additional transmission iterations could be usefult to improve the powertrain for specific mass requirements, however the '2x Kapton and Bias' design is suitable for HAMR-V and HAMR-VP.

A fifth transmission was fabricated using the SFB hip joint with a '2x Kapton

and Bias' lift DOF design and an orthogonal drive DOF. Lift DOF blocked force and free displacement were comparable to the isolated single DOF prototype, meaning the drive DOF does not contribute to serial compliance (see Figure 3.8).

3.7 Discussion

The powertrain design for the Harvard Ambulatory MicroRobot was presented in this Chapter. Theoretical and physical models for the HAMR powertrain were developed and used to select design parameters for the HAMR-V and HAMR-VP robots in Chapter 4. The work here contributed to the performance exhibited by HAMR-VP such as large sagittal plane forces that enable high speed dynamic locomotion (up to $36.9 cm/s$) and carrying additional payloads greater than $1.35g$. The PC-MEMS manufacturing process was also presented here, without which the HAMR robots could not exist at their current scale.

Chapter 4

Design and Pop-up Assembly of an Ambulatory Microrobot

4.1 Introduction

This chapter presents two quadrupedal Harvard Ambulatory MicroRobot (HAMR) designs that evolved from Hexapods in Chapter 2. The robots are the $1.07g$ Harvard Ambulatory MicroRobot V (HAMR-V), and its successor the $1.27g$ HAMR-V Pop-up (HAMR-VP). The HAMR-VP design, which implements assembly methods inspired by pop-up books, represents the capstone of this thesis. It will be the basis for all future work on ambulatory microrobots in the Harvard Microrobotics Lab, including locomotion studies in Chapter 5.

When compared to insects and other legged robots, the hexapedal HAMR prototypes demonstrated slow, quasi-static locomotion performance; the fastest recorded speed of HAMR3 was $4.3cm/s$ (0.9 body lengths per second) on perfectly flat ground,

compared to speeds up to $1.5m/s$ (50 body lengths per second) in cockroaches [15] and $2.7m/s$ (27 body lengths per second) in VelociRoach [17], the fastest walking robot normalized to body length. Therefore, a new class of Harvard Ambulatory MicroRobot has been developed: the HAMR-V robots in Figure 4.1, with the goal of achieving high-speed locomotion comparable to cockroaches and other legged robots.

The HAMR-V Pop-up (HAMR-VP), is a $1.27g$ quadrupedal microrobot whose design implements assembly techniques inspired by pop-up books to reduce manufacturing complexity and improve locomotion performance. Pop-up assembly is an advancement in PC-MEMS manufacturing, first demonstrated by Harvard Microrobotics Lab members Pratheev Sreetharan and Peter Whitney in [47]. It has since enabled the creation of complex miniature devices, such as a flapping-wing microrobot (the Monolithic Bee [43]), by reducing or eliminating difficult and tedious hand-assembly. In addition, when using pop-up assembly, tolerances are imposed by the PC-MEMS fabrication process ($1-10\mu m$) rather than a much larger variance due to the limitations of human assembly. A primary goal of implementing pop-up assembly in the HAMR robot was to exploit the enhanced tolerances to improve robot performance. Furthermore, simplifying manufacturing should make HAMR faster and easier to build, and therefore more accessible as a platform for miniature legged robotics research.

Prior to the pop-up assembled HAMR-VP, a hand-assembled version of HAMR-V was built. HAMR-V was used for maneuverability studies in Chapter 5 and a comparative analysis with HAMR-VP. In Section 4.5 of this chapter, results from low-speed quasi-static locomotion trials of HAMR-V and HAMR-VP are presented

Figure 4.1: The Harvard Ambulatory MicroRobot V series of quadrupeds includes the manually assembled $1.07g$ HAMR-V (right), pop-up assembled $1.27g$ HAMR-VP (left) and $270mg$ scaled HAMR-VP (middle).

to identify the effects of pop-up assembly on locomotion performance.

4.2 Robot Morphology and Powertrain Design

HAMR-V and HAMR-VP are nearly identical in morphology, powertrain design, and parameter selection. A quadrupedal design has been chosen to reduce manufacturing complexity over earlier HAMR prototypes, while still enabling dynamic locomotion. This choice was motivated by rapidly running insects such as cockroaches, which use quadrupedal (or even bipedal) gaits at high speeds [15]. Although not ideal for stability, having only four legs does not preclude slow speed, quasi-static locomotion in an insect-scale robot. This is primarily due to a sprawled posture, which prevents the robot center of mass from ever falling outside of a statically-stable

support region.

The HAMR-V and HAMR-VP designs utilize the flexure-based spherical five-bar (SFB) hip joint design, introduced in Chapter 3. The SFB enables two degrees of freedom (DOF) per leg: a lift DOF that raises and lowers the leg in the robot's sagittal plane, and a drive DOF that provides locomotive power in the horizontal (ground) plane. The two-DOF hip joint maps decoupled inputs from two optimal energy density piezoelectric bending bimorph actuators through flexure-based four-bar transmissions to a single leg. A study of the HAMR powertrain in Chapter 3 selected actuator and transmission parameters for HAMR-V and HAMR-VP. The sole difference between the two robots' powertrain designs is a change in HAMR-VP's drive DOF four-bar kinematics that increases stroke amplitude.

Design and manufacturing complexity is reduced in the HAMR-V series by asymmetrically coupling the drive DOFs of contralateral legs; when the front/rear left leg swings forward, the front/rear right leg swings rearward, and vice versa. This coupling scheme reduces the nominal eight DOFs to a total of six actuated DOFs: a front drive DOF, rear drive DOF, and four lift DOFs.

4.3 PC-MEMS Manufacturing

Mechanical components of HAMR-V and HAMR-VP are manufactured using the PC-MEMS fabrication paradigm [47] described in Chapter 3. While a diverse set of materials can be used with the PC-MEMS manufacturing process, components of the robots presented here consist of a five layer standard linkage laminate (SLL): a $25\mu m$ Kapton flexure at the laminate mid-plane, two rigid three-ply $[0, 90, 0]$ carbon fiber

exterior layers (YSH-50 fibers with RS-3C resin), and two sheets of acrylic adhesive (Dupont Pyralux FR-1500) to bond subsequent layers.

4.3.1 Manufacturing and Manual Assembly of HAMR-V

Hand-assembled HAMR prototypes are made from many individual PC-MEMS components; HAMR-V has 32 parts. Each of the four SFB hip joint and transmission assemblies are constructed from four SLL components (see Figure 4.2). The hip assemblies are mounted to a rigid exoskeleton, comprised of four walls of four-ply $[0, 90]_s$ carbon fiber and two custom-patterned $127\mu m$ copper-clad FR4 circuit boards. Six piezoelectric actuators are soldered at their base to the two circuit boards, providing both electrical connections and mechanical ground. Actuators are affixed at their output (tip) to their respective four-bar transmission(s) using thermoplastic adhesive (Crystalbond). The powertrain is completed with four legs that attach to the output of each SFB hip.

4.4 Manufacturing and Assembly of HAMR-V Pop-up

PC-MEMS fabrication techniques have assembly tolerances on the order of $1 - 10\mu m$, and therefore prototype fidelity is highly dependent on the complexity and number of manually-assembled components. Therefore, as mentioned in Section 4.1, implementing pop-up assembly in the design of HAMR-VP is primarily motivated by the following goals: a) improving manufacturing tolerances and thus locomotion

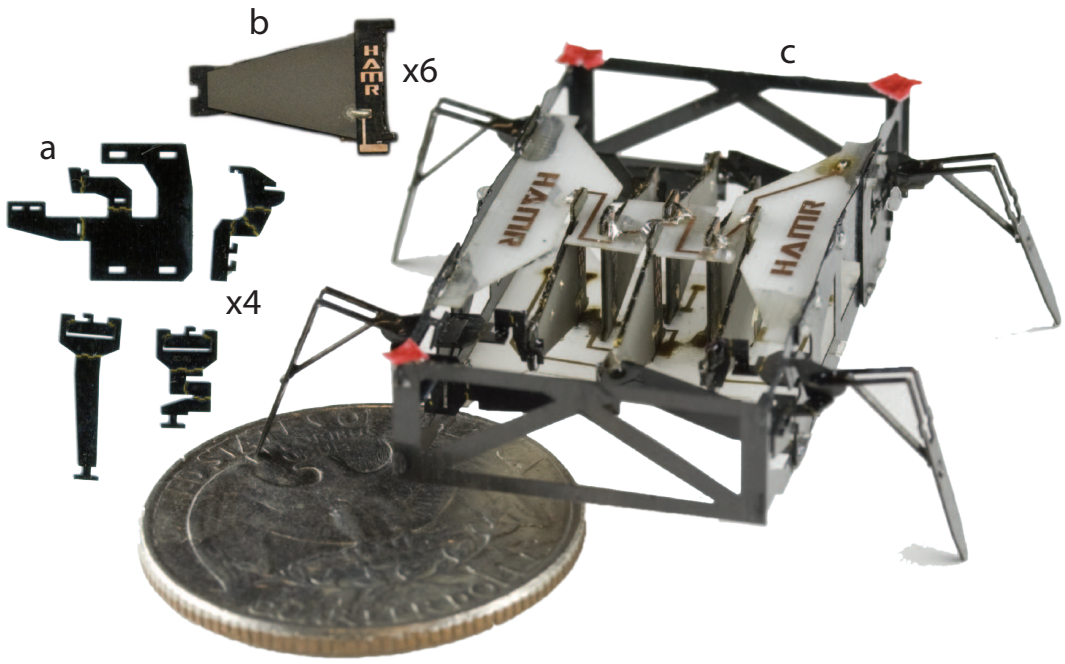

Figure 4.2: Components of HAMR-V. Two Standard linkage laminate (SLL) components are manually assembled to create each spherical five-bar hip joint, and two additional components form the input four-bar transmissions (a). Mechanical power is generated by six piezoelectric bending bimorph actuators (b); four control the lift DOFs and two control drive. Additionally, four $[0, 90]_s$ carbon fiber laminates and two copper-clad FR4 circuit boards form the robot exoskeleton. All components are hand-assembled to produce the HAMR-V robot (c).

performance, and b) making the HAMR platform more accessible to other researchers by reducing manufacturing complexity. In one extreme, pop-up techniques enable complex mechanisms that emerge from a single laminate [47], [43]. However unlike those devices, the HAMR-VP design does not implement a fully monolithic assembly process; it has 13 components to allow modularity of actuators and legs, two topics of concurrent research.

Laminate Composition Designing HAMR-VP with pop-up assembly requires an expansion of the five-layer SLL described in Section 4.3. The design uses 23 material

layers, which compose four standard linkage sub-laminates (five layers each). Subsequent linkage sub-laminates are bonded using tack-bonded acrylic adhesive (three layers), a bonding process that enables small "islands" of adhesive rather than continuous sheets [47]. See Figure 4.3 for a cross-sectional view of the HAMR-VP laminate composition.

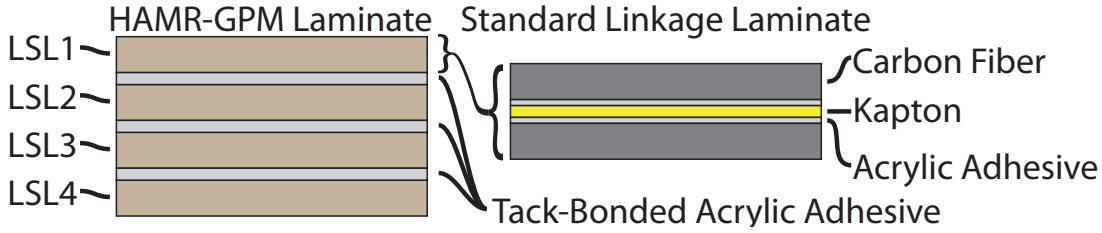

Figure 4.3: The HAMR-VP laminate stack consists of 23 material layers: four standard linkage sub-laminates (five layers each) and three layers of tack-bonded adhesive to bond subsequent linkage laminates.

Spherical Five-Bar Sub-Laminates (LSL1 and LSL4) The pop-up HAMR-VP design utilizes the monolithic spherical five-bar joint design from [43] and [44]. This SFB design can be fabricated from a single linkage laminate, rather than from two components as in HAMR-VP (see Figure 4.4). Thus, manufacturing tolerances are improved and assembly is easier than described in Section 4.3.1. Kinematically, HAMR-VP's SFB hips behave identically to those described above for HAMR-V, however each hip only requires one 90° fold to deploy the two links that couple the lift and drive DOFs. Each SFB is folded manually during final assembly of the robot, but this is trivialized by features that constrain joint limits to exactly 90°.

In the HAMR-VP material layup, two outer linkage sub-laminates labeled LSL1 and LSL4 are comprised of the four spherical five-bar hip joints. The laminate is

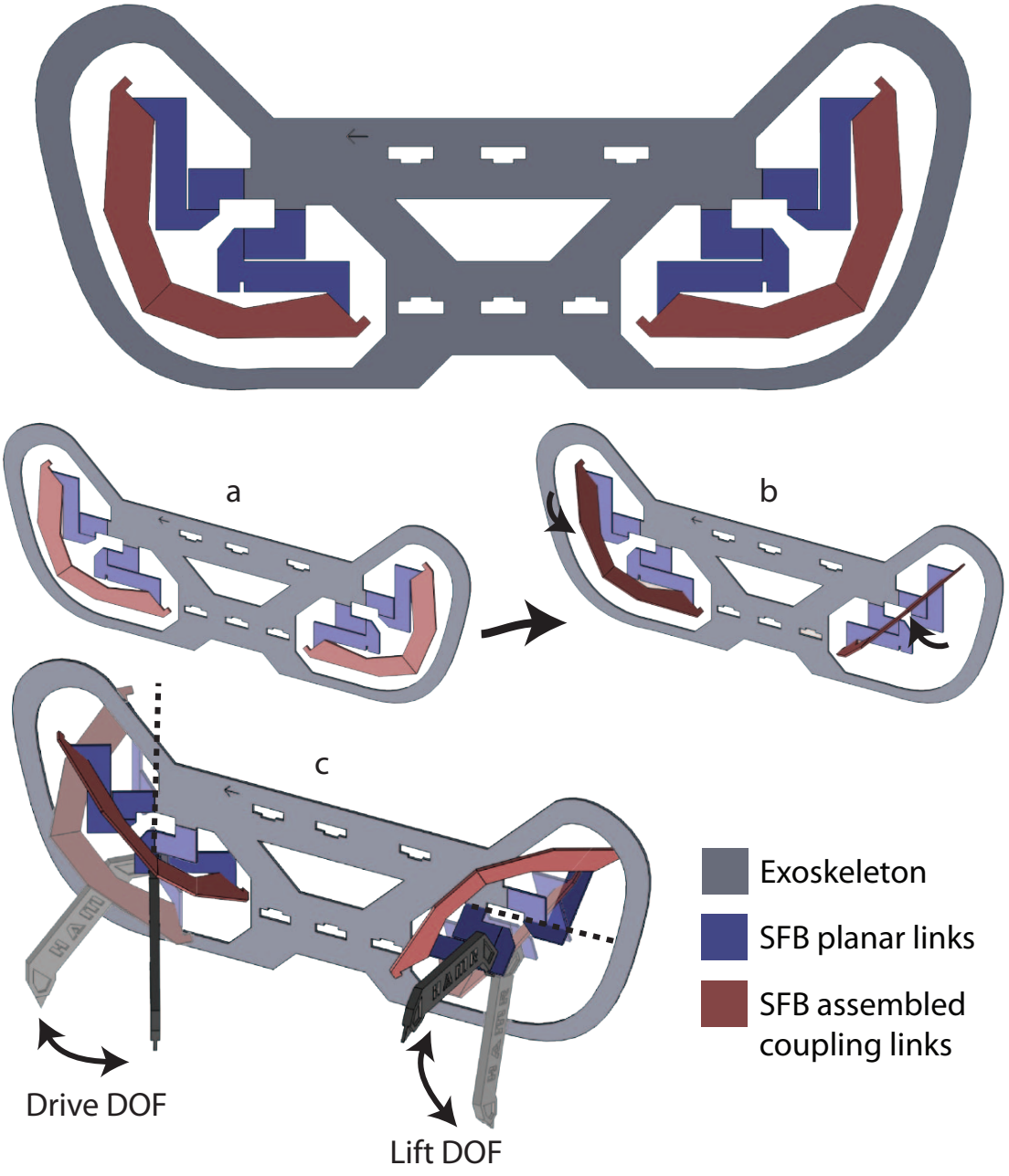

Figure 4.4: HAMR-VP uses a monolithic spherical five-bar (SFB) hip joint design introduced in [43]. The outer linkage sub-laminates of HAMR-VP, LSL1 and LSL4, are composed of the four SFBs. Here, LSL4 and its two SFBs are shown as a flat laminate (a), after deployment by a 90° fold (b), and with two legs to diagram the lift and drive DOFs (c).

orientated such that the robot pops-up laterally, meaning the center of the material laminate (layer 13 of 23) is also the robot sagittal midplane. Therefore, LSL1 (the robot's right side) and LSL4 (the robot's left side) are symmetric.

Input Four-bar and Pop-up Strut Sub-Laminates (LSL2 and LSL3) Linkage sub-laminates LSL2 and LSL3, also symmetric about the robot mid-plane, are comprised of the eight four-bar transmissions between each actuator and SFB, folding struts for popup assembly, and additional assembly features (see Figure 4.5). Four-bar transmissions are adhered to the SFB via tack-bonded acrylic adhesive. Each four-bar transmission is deployed with a simple 90° fold, similarly to the SFBs, and mated to its respective actuator output during final assembly.

Three parallel assembly struts effectively form a sarrus linkage, enabling pop-up assembly of HAMR-VP by allowing separation of the right (LSL1 and LSL2) and left (LSL3 and LSL4) halves of the robot in a single DOF (see Figure 4.5). The assembly linkages constrain the pop-up motion such that LSL1 and LSL4 remain parallel and traverse a straight line during assembly. The robot is deployed when the assembly struts become fully extended and are orthogonal to LSL1 and LSL4. Each strut is fixed on either end to the outer linkage sub-laminates (LSL1 to LSL2 and LSL4 to LSL3), and at the laminate mid-plane (LSL2 to LSL3) using tack-bonded acrylic adhesive.

Laminate Manufacturing Process The manufacturing process for HAMR-VP (see Figure 4.6) begins by machining the 23 material layers using a diode-pumped solid state (DPSS) laser, followed by pin-alignment and stacking on a jig. The laminate is

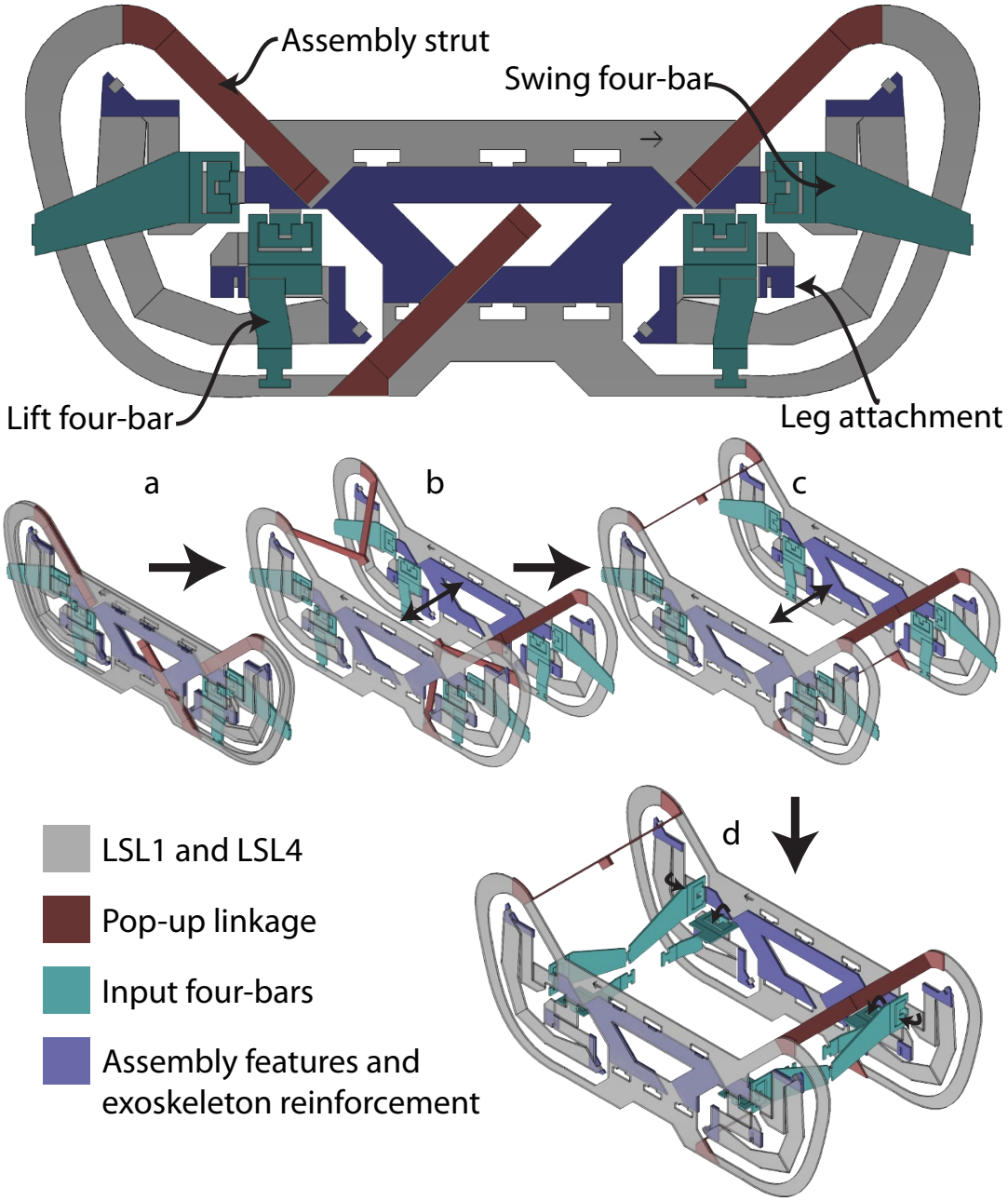

Figure 4.5: Sub-laminates LSL2 and LSL3 comprise the pop-up assembly linkages, four-bar transmissions, and additional assembly features. The released pop-up linkage assembly (a) allows separation of the two robot halves, LSL1 and LSL4 (b,c). After pop-up assembly, the eight input four-bars are deployed by 90° folds (d).

cured under heat and pressure, then the robot outline and pop-up DOF are released from the surrounding material using the DPSS laser.

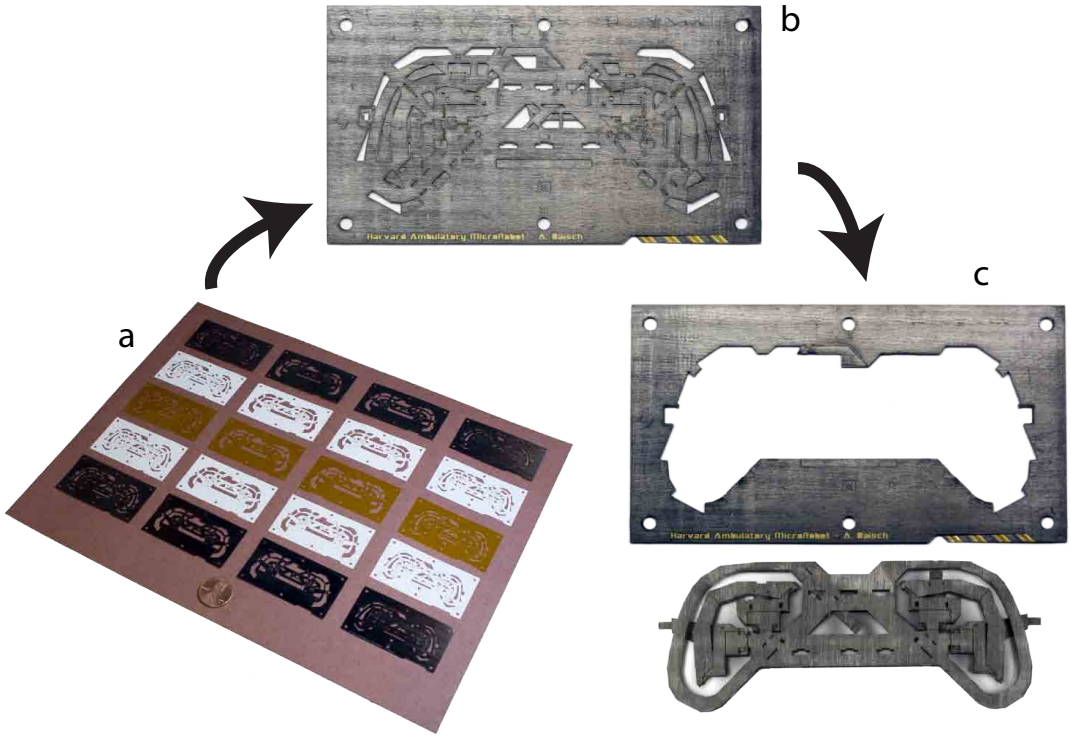

Figure 4.6: Manufacturing process for the pop-up HAMR-VP. 23 material layers, 20 continuous sheets (a) and 3 tack-bonded adhesive layers, are laser machined and laminated to produce (b). A second laser-machining step releases the HAMR-VP structure (c), allowing initial pop-up assembly.

Final Assembly Once released, completion of HAMR-VP requires manual assembly of the 13 components (see Figure 4.7). First, the exoskeleton is completed by fully expanding the pop-up DOF and inserting two copper-clad FR4 circuit boards, which trace off-board power and control electronics to the actuators. The circuit boards are populated with six piezoelectric cantilever actuators, using solder as a mechanical and electrical interface. Each input four-bar transmission is then assembled by making a

90° fold and affixing its input link to the output (tip) of its respective actuator. The robot is completed once spherical five-bar coupling links are folded 90° to their joint stop, and four legs are attached to the hip joints. As previously mentioned, legs and actuators are modular, and therefore the leg-to-hip and actuator-to-four-bar bonds are made using a thermoplastic adhesive. All other bonds, such as at 90° transmission folds, are made with permanent cyanoacrylate glue.

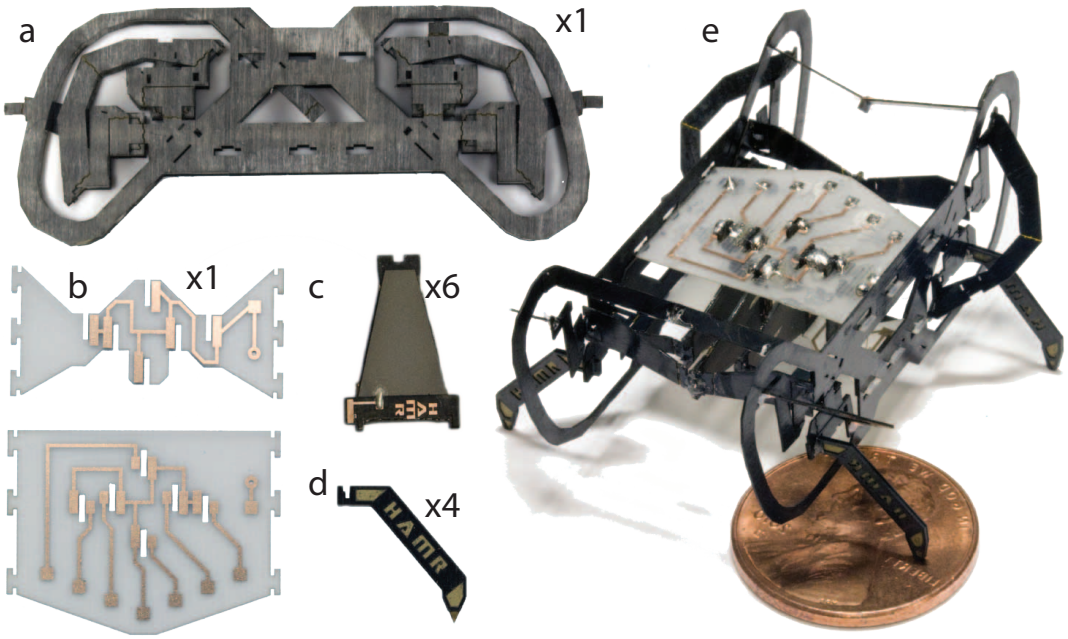

Figure 4.7: The HAMR-VP pop-up laminate (a) is fully opened and constrained with two copper-clad FR4 circuit boards (b). The circuit boards, which trace from off-board power and control electronics, are populated with piezoelectric actuators (c) using solder for electrical and mechanical connection. Four-bar transmissions and SFBs are deployed, followed by attaching four legs (d) to their respective SFB output to finalize assembly of HAMR-VP (e).

4.5 Results

HAMR-VP was successfully manufactured, making it the the first mechanism capable of locomotion made using PC-MEMS with pop-up assembly. To evaluate the hypothesis that performance would improve with tighter assembly tolerances (attributed to popup assembly), a manually-assembled HAMR-V was fabricated for a comparative analysis of locomotion performance.

Although HAMR-VP was designed to be a high-speed, dynamic robot, it is capable of quasi-static locomotion on flat ground. Extensive high-speed locomotion performance analysis is the subject of Chapter 5. The results presented here are at low gait frequencies below $10Hz$.

4.5.1 Comparative Quasi-Static Locomotion Performance

At low gait frequencies, HAMR-V and HAMR-VP were evaluated in straight locomotion speed and energetics, maneuverability, and payload capacity. Results were obtained in the two-dimensional walking plane using overhead video from a Pixelink camera and custom postprocessing software that tracks the robot's center of mass and orientation.

Initial tests of all gait parameters in HAMR-V led to selection of a low speed trotting gait; a two-beat gait where diagonal pairs of legs (i.e. front-left and rear-right or front-right and rear-left) propel the robot forward simultaneously. Due to the instability of a bipod, at low speeds the robot settles to a stable third leg during part of each step. The fastest quasi-static locomotion speeds were obtained for both robots with drive DOFs exactly 180° out of phase and lift DOFs beginning their descent to

the ground 90° before their respective drive DOF begins driving rearwards.

Reported values in Figure 4.8 represent the forward velocity of the robot (as defined by a body-fixed coordinate frame) during straight locomotion, which ignores lateral and rotational motions. The only difference between robot trials is the input waveform used: in HAMR-V, a ramped square (trapezoidal) wave is used to generate the highest actuator force per stride, and thus highest speed. In HAMR-VP, sine wave inputs are used; trapezoidal inputs cause erratic behaviour at frequencies above $4Hz$, due to resonant frequency excitation in the under-damped powertrain (ringing) that causes each foot to strike the ground more than once per stride. The results show that HAMR-VP exceeds the velocity of HAMR-V by an average factor of 2.4 at comparable frequencies below $10Hz$. The measured difference in velocity reached a maximum factor of 3.0 at $2Hz$ and minimum of 1.2 at $4Hz$.

Tethered, straight locomotion energetics were evaluated by measuring electrical power delivered to the six piezoelectric actuators. At trials from $0.5 - 10Hz$, HAMR-VP and HAMR-V required on average $11mW$ and $12mW$, respectively. Cost of transport is commonly defined as as the work (E) required to move a mass (M) a distance (D), or $COT = E/(MD)$ or equivalently $COT = P_{avg}/(V_{avg}M)$. Due to a lower velocity and mass, HAMR-V has an average cost of transport 3.2 times greater than HAMR-VP averaged over all trials from $2 - 10Hz$.

Payload capacity was evaluated by measuring robot walking speed while carrying one to six additional $225mg$ masses (see Figure 4.9). On flat ground, HAMR-V failed to walk with greater than $900mg$ additional payload. HAMR-VP successfully walked with a $1350mg$ payload at speeds greater than HAMR-V with no payload.

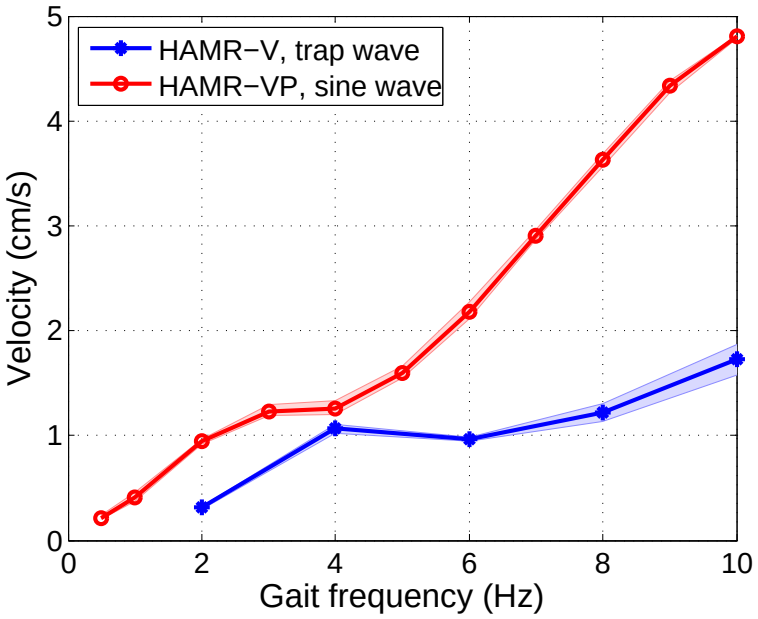

Figure 4.8: Speed results from quasi-static locomotion of HAMR-V and HAMR-VP. Reported speed is the mean velocity in the direction of the robot heading, which discounts lateral drift and rotation associated with unstable quasi-static quadrupedal gaits. Error bars represent maximum and minimum speed across three trials.

4.5.2 Comparative Quasi-Static Trajectory Stability and Maneuverability

In Chapter 5, control schemes to turn the HAMR-V robot will be presented. As a result of those maneuverability studies, we determined that the simplest effective control parameter for quasi-static locomotion of the HAMR-V robots is ϕ_i $(i = 1, 2, 3, 4)$, defined as the phase between a leg's lift DOF driving down to the ground, and drive DOF driving rearward to propel the robot. Increasing/decreasing ϕ_i causes leg i to touch down later/earlier than its diagonal biped counterpart, thus rotating the robot body.

In HAMR-V and HAMR-VP, turning was performed using ϕ_1 of the front left leg

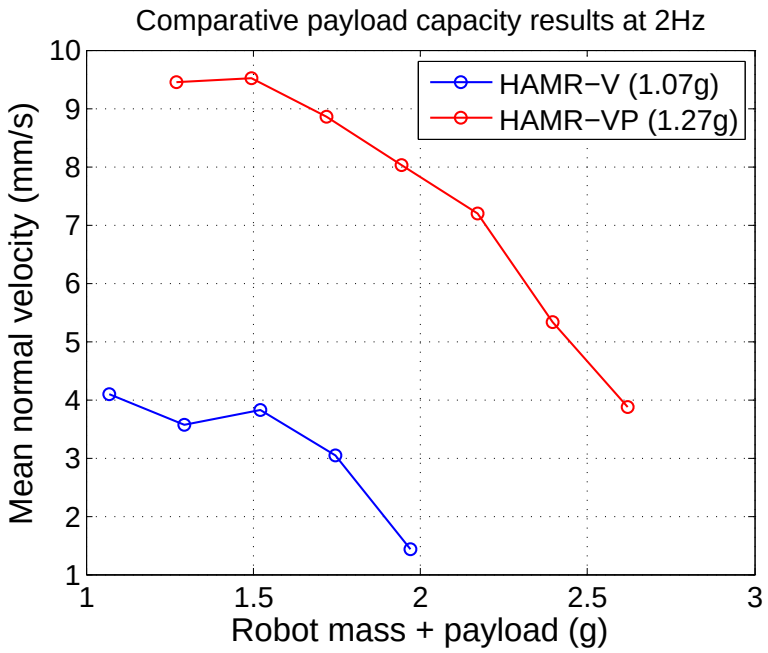

Figure 4.9: Payload capacity of $1.07g$ HAMR-V and $1.27g$ HAMR-VP on flat ground. Robot velocity was measured with up to an additional $1.35g$ using discrete $225mg$ masses. At low frequencies, HAMR-V is unable to move with greater than $900mg$ of additional mass. Representative results are shown at $2Hz$ gait frequency, but were consistent from 1-10Hz.

as a feedforward control parameter. Turning trajectories and final robot orientation at $2Hz$ gait frequency are presented in Figure 4.10 for $\phi_1 = 30, 60, 90, 120, 150$. There are various methods to quantify maneuverability during ground locomotion. Two possible metrics include average angular velocity and turning radius; higher velocity and smaller turning radius are characteristics of faster turns. Using these metrics, HAMR-V and HAMR-VP perform nearly identically in turning rate, however HAMR-V exhibits a smaller turning radius.

Another method to measure stability in maneuverability is presented in [14], which defines a successful turn as one that simultaneously deflects average heading (the direction of average COM velocity) and changes orientation such that the robot's body

axis remains aligned with its heading. In walking robots, a large variance between robot heading and orientation necessitates additional onboard sensing and control for successful turns. At HAMR-V's scale, additional components come at a large cost to payload and power. Across all trials in Figure 4.10, HAMR-VP outperformed HAMR-V with average heading-to-orientation deviations of 11° to 29°, respectively.

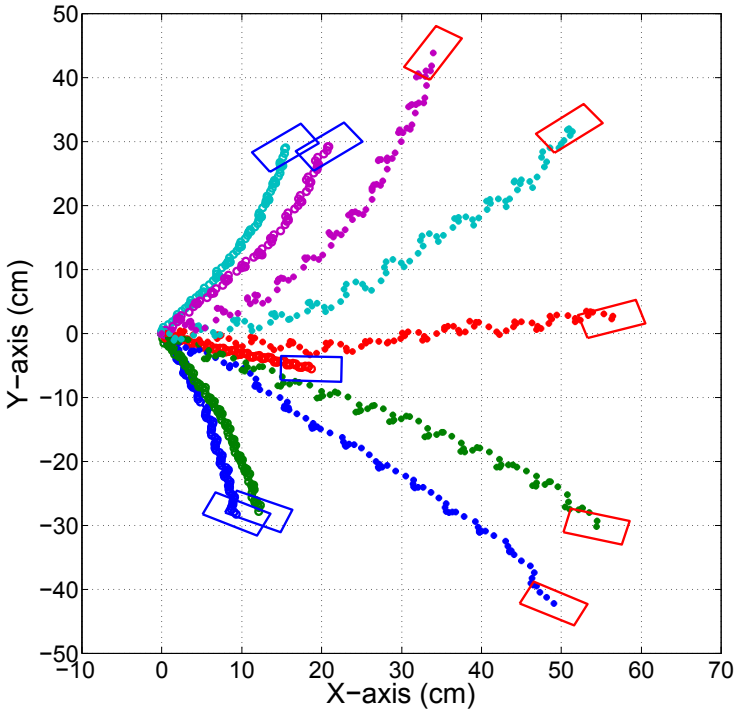

Figure 4.10: Maneuverability results using ϕ_1 as a feedforward control input at $2Hz$ gait frequency over $6s$ trials. Robot trajectories are presented for $\phi_1 = 30°$ (hard right turn), $\phi_1 = 60°$ (shallow right turn), $\phi_1 = 90°$ (straight), $\phi_1 = 120°$ (shallow left turn), and $\phi_1 = 150°$ (hard left turn). The robot's orientation at the end of each trial is represented by a blue (HAMR-V) or red (HAMR-VP) rectangle.

4.5.3 Design Scaling

A primary goal of implementing pop-up assembly in HAMR was to make the platform more accessible to other researchers. Evaluating the success of HAMR-VP in this regard is impossible in the short term. However, a similar metric is whether the implementation of pop-up assembly enables instantiation of designs too-small or complex for manual assembly. Therefore, a smaller version of HAMR-VP was created by photographically scaling its two-dimensional CAD drawings by a factor of 0.5. The result is a $270mg$ quadruped capable of tethered, flat-ground locomotion (see Figure 4.1).

4.6 Discussion

The design of HAMR-VP, a $1.27g$ quadrupedal microrobot manufactured using the PC-MEMS fabrication paradigm and pop-up assembly techniques, has been presented here. To quantify the effect of implementing pop-up assembly into a HAMR design, quasi-static locomotion results were compared to HAMR-V, a $1.07g$ hand-assembled robot with nearly identical design parameters. The results of this comparison suggest that designing HAMR for pop-up assembly improved walking speed, efficiency, payload, and maneuverability.

In quasi-static straight line speed trials from $1 - 10Hz$, HAMR-VP outperformed HAMR-V by an average factor of 2.4 across comparable gait frequencies. Due to HAMR-V's lower mass and speed but similar power requirements, its average cost of transport was 3.2 times greater than HAMR-VP. Although the increase in velocity

could be attributed to a change in drive DOF kinematics, an improvement in flat-ground payload capacity suggests that despite identical design parameters, HAMR-VP has a greater power output in the lift DOF. In maneuverability trials, HAMR-V and HAMR-VP demonstrated similar turning rates, however HAMR-VP showed significantly better performance in turn stability.

Furthermore, a $270mg$ quadruped capable of tethered flat ground locomotion was presented. This robot, along with other work [47], [43], [44], demonstrate a variety of complex miniature devices achievable only by implementing pop-up assembly into PC-MEMS manufactured devices. The locomotion performance results presented here suggest that implementing pop-up assembly into PC-MEMS devices simultaneously improves mechanism performance and increases achievable mechanism complexity.

In Chapter 5, locomotion studies show that the current instantiation of HAMR-VP can reach speeds up to $36.9cm/s$. Outside of this work, HAMR-VP has become a platform for additional research in a variety of fields including implementation of on-board electronics, feedback control using onboard sensing, and additional locomotion studies to improve performance.

Chapter 5

Locomotion Studies

5.1 Introduction

This chapter presents locomotion studies performed on the quadrupedal Harvard Ambulatory MicroRobot-V Pop-up (HAMR-VP) presented in Chapter 4. Results include performance in two regimes: a 'quasi-static' regime and a 'dynamic' regime referring to the use of powertrain dynamics to increase per-stride energy. Highlights of the HAMR-VP locomotion results include running up to $36.9cm/s$ (8.4 body lengths per second in the $4.4cm$ long HAMR-VP) at $50 - 70Hz$ gait frequency and payload capacity of $1.35g$. Additionally, designs for high-friction feet and their effect on locomotion are presented. Lastly, walking-plane maneuverability is investigated, and a single parameter for heading control is found.

Biological studies have concluded that running animals exceed their quasi-static maximum velocity through the use of body dynamics [1]; compliant elements distributed throughout their musculoskeletal structure allow aerial phases, thus break-

ing kinematic constraints. Many legged robots, constrained by actuator bandwidth, use a biologically inspired approach to achieve high-speed dynamic gaits. By designing compliant elements into the robot's legs or transmissions, a number of robots have achieved speeds exceeding quasi-static maxima at their gait frequency, including: VelociRoACH [17], DASH [8], Sprawlita [10], RHex [40], and Boston Dynamics's Cheetah Robot [11]. Elastic elements can additionally improve energy efficiency [1], minimize gait control [42], enhance obstacle avoidance [39], and add shock absorption [1], [8], [38]; characteristics worth implementing into HAMR in the future. However, an alternative approach is taken in this work to simply increase locomotion speed above the quasi-static limit by utilizing the high bandwidth and quality factor characteristics of the HAMR powertrain.

5.2 Quasi-Static Locomotion

In this section, HAMR-VP's locomotion below $10Hz$ gait frequencies is characterized. The results in this section show that this locomotion is quasi-static; legs take discrete steps, and velocity is bounded by the product of stride length and frequency. This performance regime, thoroughly defined when examining the powertrain frequency response in Section 5.4, was defined by a roughly linear relationship between frequency and speed. Above $10Hz$, powertrain dynamics affected this relationship and required modified actuator inputs, as later discussed in Section 5.5. To begin this section, a parameterization of HAMR-VP's actuator inputs and gait is presented, followed by locomotion results at gait frequencies below $10Hz$.

5.2.1 Input Parameterization and Walking Gait

Each of HAMR-VP's piezoelectric actuators is voltage-driven using an alternating drive configuration consistent with [25], thus requiring bias, ground, and signal voltages. To simplify electrical inputs, all six actuators share a single bias and single ground rail. Therefore, eight unique voltages are required for the robot: constants V_{Bias} and ground, and six drive signals, V_{s1-6}. Voltages are generated by off-board electronics, using a controller written in Matlab and Simulink and interfaced with an xPC Target real-time testing environment. Bias and control signals are then amplified to high voltages (up to $250V$) and fed to the piezoelectric actuators by 52-gauge copper wire.

In versions prior to HAMR-VP, trapezoidal inputs were used to drive HAMR's piezoelectric actuators; a pure square wave would result in maximum ground contact per actuator cycle; however, high slew rate input signals could damage the piezoelectric ceramic. In HAMR-VP, trapezoidal inputs combined with an under-damped powertrain and rigid carbon fiber feet caused: 1) elastic collisions between the foot and ground, 2) oscillations at the apex of each step (ringing) and 3) slipping between the foot and ground. Therefore, only sinusoidal inputs were used to prevent stochastic behavior.

Sinusoidal inputs to HAMR-VP are defined $V_{si} = V_{0i} + \frac{V_{ai}}{2}\sin(2\pi f_i t + \psi_i)$ with parameters: mean voltage V_0, peak-to-peak amplitude V_a, frequency f, and phase ψ_i. In Chapter 4, ϕ_i was defined for leg i as the phase offset between where the lift DOF begins moving downward and drive DOF begins moving rearward. See Figure 5.1c for the relationship between ϕ_i and ψ_i. Input parameter subscripts are equivalent to

their affected leg(s) according to the convention in Figure 5.1a; independent lift DOF signals are $V_{s1}, V_{s2}, V_{s3}, V_{s4}$ and coupled drive signals are V_{s12}, V_{s34}.

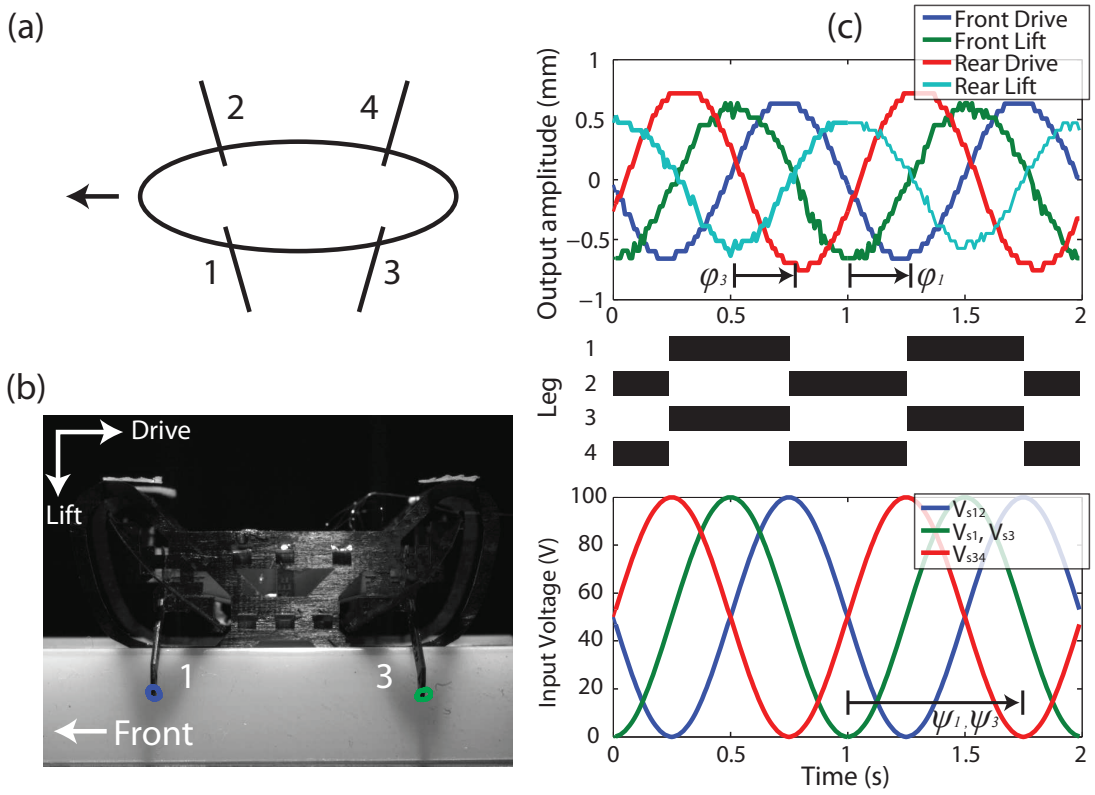

Figure 5.1: HAMR-VP's actuator input and leg convention. Six actuators are driven by sinusoidal inputs $V_{si} = V_{0i} + \frac{V_{ai}}{2}\sin(2\pi f_i t + \psi_i)$ (c). Parameter subscripts indicate the leg(s) that each actuator affects, using the convention in (a). Two 90° out of phase sinusoidal inputs to the lift and drive DOFs (c) cause a roughly circular output (b). Actuating the front and rear drive DOFs 180° out of phase causes a gait similar to a trot (c), although here is used for quasi-static operation as well; black bars in (c) represent the footfall pattern of HAMR-VP's nominal gait. Due to symmetry between front and rear lift powertrains (actuators face in opposite directions), in-phase lift DOF inputs to legs 1 and 3 have outputs 180° out of phase (c).

For straight locomotion, the parameter space was reduced from 25 (V_{Bias} and six actuators with four parameters each) to 12 by enforcing symmetry between the front/rear and left/right sides of the robot. The twelve input parameters for straight locomotion are summarized in Table 5.2.1. Nominal parameter values were chosen

for a walking gait similar to a trot. Drive inputs were therefore 180° out of phase to generate in-phase diagonal legs with a footfall pattern shown in Figure 5.1c. A quick study varying lift input phase found the fastest locomotion at $\psi_1 = \psi_2 = \psi 3 = \psi_4 =$ 270°, and was therefore chosen as the nominal value.

Table 5.1: Input Parameters for Straight Locomotion

Parameter	**Description**	**Nominal Value**
V_{Bias}	Actuator bias voltage (V)	$200V$
f	Gait frequency (Hz)	$1 - 98Hz$
V_{0-Li}	Lift DOF signal mean (V)	$100V$
V_{a-Li}	Lift DOF signal peak-to-peak amplitude (V)	$200V$
V_{0-Dr}	Drive DOF signal mean (V)	$100V$
V_{a-Dr}	Drive DOF signal peak-to-peak amplitude (V)	200V
$\psi_{1,2,3,4}$	Lift signal phases ($degrees$)	270°
ψ_{12}	Front Drive DOF phase ($degrees$)	180°
ψ_{34}	Rear Drive DOF phase ($degrees$)	0°

5.2.2 Speed, Power, and Payload Results

In Chapter 4, comparative quasi-static locomotion results below $10Hz$ gait frequency were presented to identify the positive effects of implementing pop-up assembly into the design of HAMR. HAMR-VP's performance is reiterated here as part of the discussion of quasi-static verses dynamic locomotion. A sweep of phase parameters led to the fastest speeds using nominal values in Table 5.2.1. The maximum frequency used in this section is $10Hz$, above which powertrain dynamics affect locomotion; Section 5.4 explores gait frequencies above $10Hz$.

The experimental setup used to obtain quasi-static locomotion results consisted of a card stock walking surface and overhead camera (PL-B741F, Pixelink). Three markers on the robot were tracked using custom post-processing software developed

by Dr. Onur Ozcan to obtain robot center of mass position (x, y) and orientation (Θ). Velocities were obtained by numerical differentiation of position and orientation with respect to time.

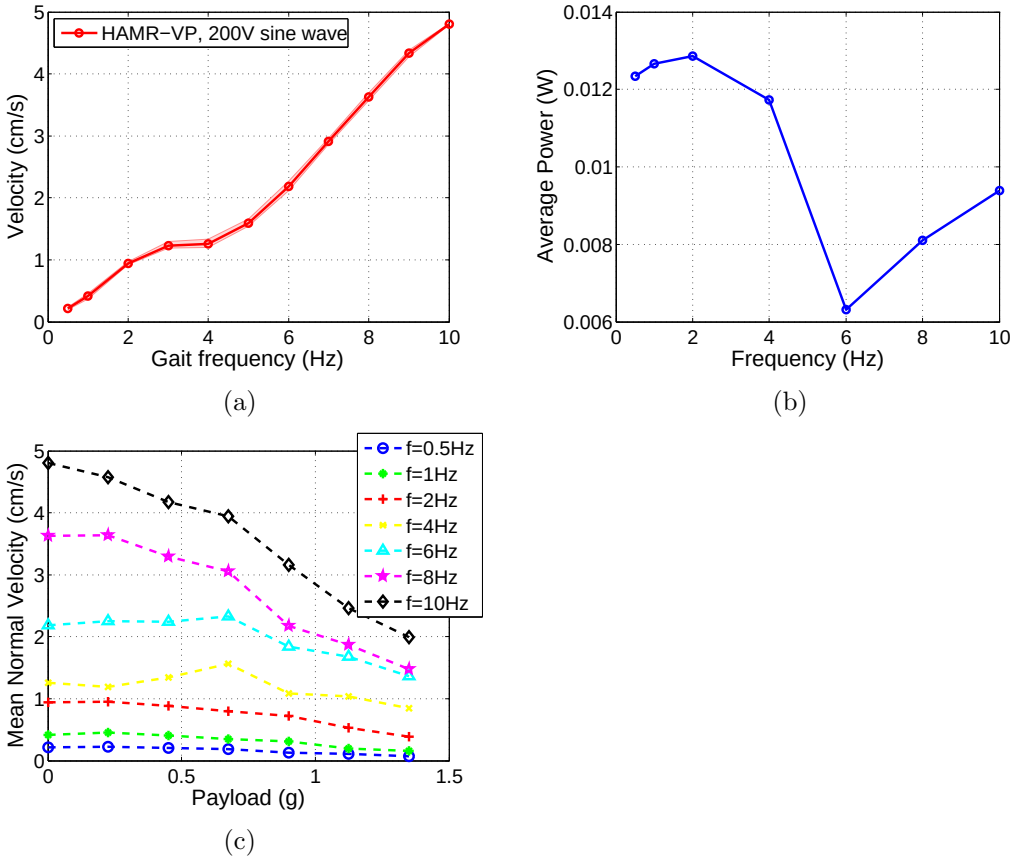

Figure 5.2: Straight, quasi-static locomotion results of HAMR-VP. Trials were conducted from 1-10Hz, recording speed (a) and electrical power consumption (b). Data in (a) represents average trial velocity, defined by a body-fixed coordinate frame (ignoring lateral and rotational movement). Error bars in (a) indicate maximum and minimum velocity across three trials; note the consistency of results. Additionally, payload capacity was measured by adding discrete $225mg$ masses to the back of HAMR-VP and recording velocity (c).

Figure 5.2 summarizes locomotion performance in the quasi-static regime. Speed measurements in Figure 5.2a represent average forward velocity (as defined by a body-fixed coordinate frame) ignoring lateral and rotational motions. The results

show a nearly linear relationship between frequency and velocity, excluding a small deviation from 4-6Hz. The slope of a linear fit to this data approximates the per-cycle displacement of $4.8mm$ ($2.4mm$ per step). The linear fit represents a quasi-static speed limit for HAMR-VP. The goal of work in the dynamic regime will be to exceed this trend.

Electrical power of all six actuators was measured during locomotion and plotted in Figure 5.2a. Average power at $1-10Hz$ gait frequencies ranged from $6.3mW$ at $6Hz$ to $12.9mW$ at $2Hz$ with a mean of $10.5mW$. Power measurements were also taken with the robot elevated from the walking surface with no effect on results. Comparing these power measurements to animals and other vehicles requires knowledge of onboard high-voltage electronics power consumption and efficiency, which can be attained once onboard electronics are developed for HAMR-VP.

The effects of payload on locomotion were obtained by adding discrete $225mg$ masses to the back of HAMR and measuring locomotion speed (see Figure 5.2c). HAMR-VP was tested with up to $1350mg$ additional payload, where the locomotion mechanism became stick-slip; feet did not leave the ground, but reduced friction in swing phase legs enough to cause net forward locomotion. At this point only walking on perfectly flat ground would be possible. Estimated mass of a design for onboard electronics and battery (contributed by Dr. Mike Karpelson) is $600-700mg$. Results with $675mg$ payload generally show a $6-18\%$ decrease in quasi-static velocity, except at 4 and $6Hz$. The velocity increase at 4 and $6Hz$ is likely due to increased foot-ground friction caused by an increase in normal force, coupled with a change in body dynamics discussed in Section 5.4. The quasi-static payload results suggest that there

exists an optimum robot mass, at which increased foot-ground friction overcomes any reduction in speed contributed by additional payload.

5.3 Modifying Foot-Ground Friction and its Effect on Locomotion

In quasi-static locomotion studies, low friction between HAMR's carbon fiber feet and the card stock substrate caused slipping, preventing the use of higher energy (e.g. trapezoidal) input signals. In the payload study above, results indicated that normal force from additional payload improved foot-ground friction, thus increasing locomotion speed. An alternative to increasing robot mass is affecting foot-ground friction with material and contact area. Therefore, a manufacturing technique was developed to create molded polymer feet compatible with HAMR's carbon fiber PC-MEMS legs. A simple set of the resulting feet were used to investigate the effect of foot-ground friction on quasi-static locomotion.

5.3.1 Foot Design and Manufacturing

In order to increase foot-ground friction during locomotion, a process was developed to mold soft polymer feet to the distal end of each HAMR leg (see Figure 5.3). Legs are pre-manufactured from five layers using the PC-MEMS process; three 8-ply $[0, 0, 90, 90]_s$ carbon fiber laminates (YSH-50 fibers, RS-3C resin), and two acrylic adhesives to bond subsequent layers (FR-1500, Dupont). Each leg is terminated by a rounded tip with through-holes that allow polymer linking across the carbon fiber

thickness; this increased strength over relying on bonds between inert silicone rubber and carbon fiber.

Feet with arbitrary 2.5D shapes could be produced using a variety of molds. Here, 3D-printed molds were rapidly prototyped from Vero (rigid) materials on the Connex 500 (Objet). Feature resolution using the Connex 500 was limited to approximately $100-300\mu m$; to improve resolution, alternative molding techniques using conventional machining, soft lithography [52], or micro-molding [18] could easily be implemented. Two-part rubbers, ranging from soft urethane (VytaFlex Shore 30A, Smooth-On Inc.) to softer silicone (EcoFlex Shore 00-30, Smooth-On Inc.) were used in molded foot prototypes. Additional polymers could be used, however high pre-cured material viscosity might limit feature resolution.

The manufacturing process begins by pouring mixed two-part rubbers into the mold cavities, followed by planarization to remove excess liquid. An array of pre-cut legs is then suspended with their feet inside the mold cavity. Uncured polymer is degassed under vacuum, followed by room temperature curing based on material specifications. The curing process can be accelerated by baking at elevated temperatures, not exceeding $60°C$ to prevent warping of the 3D-printed molds. Rubber feet are easily removed from the mold with 100% yield. Occasionally, flashing must be removed using fine tweezers or a razor blade. Finally, individual legs are singulated using a $355nm$ UV laser. Several resulting mold and feet geometries are shown in Figure 5.3.

The effects on locomotion of increased friction and adhesion due to molded soft polymer feet is explored below. Additionally, future work could use this manufactur-

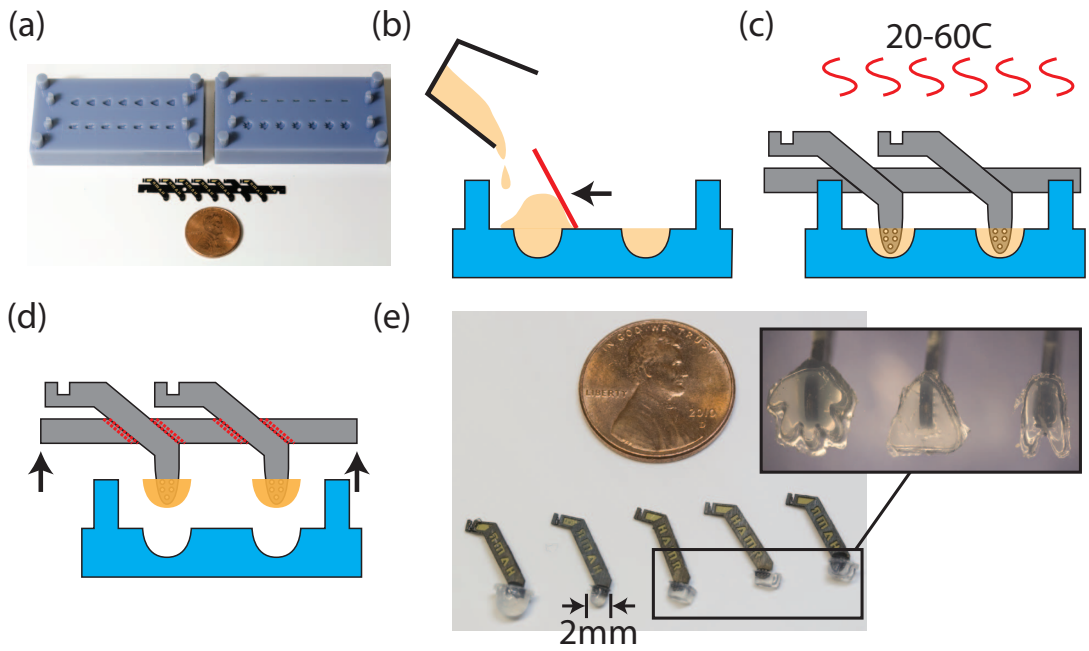

Figure 5.3: A molding process was developed to implement structured soft rubber feet onto HAMR-VP's PC-MEMS manufactured legs. The process begins with a pre-cut array of carbon fiber legs and 3D-printed mold (Connex 500, Objet) (a). Two-part rubbers are poured into the mold cavity, followed by planarization to remove excess and degassing under vacuum (b). Legs are then suspended above the mold cavity, with their distal ends submerged in polymer, and cured at room temperature overnight or at an accelerated rate at elevated temperatures (up to $60°C$) (c). Finally, the array is removed from the mold and singulated using a $355nm$ UV laser (d), producing legs and feet with arbitrary 2.5D geometries (e).

ing process to implement tuned leg stiffnesses and develop adhesive feet for traversing inclined, vertical, and inverted surfaces similar to gecko-inspired fibrillar adhesives [33], [29], [3].

5.3.2 Locomotion Results

HAMR-VP was equipped with a set of legs with $2mm$ hemisphere soft (Shore 0030, below the Shore A scale) silicone rubber (EcoFlex, Smooth-On Inc.) feet (see

Figure 5.3e). Quasi-static locomotion was studied, similar to Section 5.2, and normal, lateral, and angular velocities were compared to those using rigid carbon fiber feet. Foot-ground friction was characterized using the single leg setup described in Chapter 3. Experiments consisted of displacing the passive powertrain down towards the ground, measuring reaction vertical and lateral friction force on the foot. The results show a significant increase in lateral force between plain carbon fiber and EcoFlex feet. Actual data values were susceptible to artifacts of static friction using the EcoFlex feet; the feet did not slip, thus normal and lateral forces were balanced. Although accurate values cannot be reported, the results are a clear indication that EcoFlex feet substantially increase foot-ground friction over carbon fiber feet.

Legs with soft polymer feet were implemented on the HAMR-VP robot to compare quasi-static locomotion performance to carbon fiber feet on a card stick surface (see Figure 5.4). Results showed that forward velocity was comparable in both systems using the same sinusoidal gait inputs. As mentioned in Section 5.2, slipping and elastic collisions between the carbon fiber foot and ground precluded the use of higher energy waveforms (e.g. trapezoidal). Soft polymer feet prevent this behavior by adhering to the ground during each step and enable the use of $200V$ trapezoidal inputs, which increase locomotion speeds $17 - 56\%$ compared to sinusoids.

In addition to enabling higher speed quasi-static locomotion, EcoFlex feet improved lateral and rotational instability. Figure 5.4b,c show that lateral and angular velocities decreased with the implementation of soft polymer feet for sinusoidal inputs.

In Section 5.4, high speed locomotion is enabled by high gait frequencies using plain carbon fiber feet. In an attempt to compare results between carbon fiber and

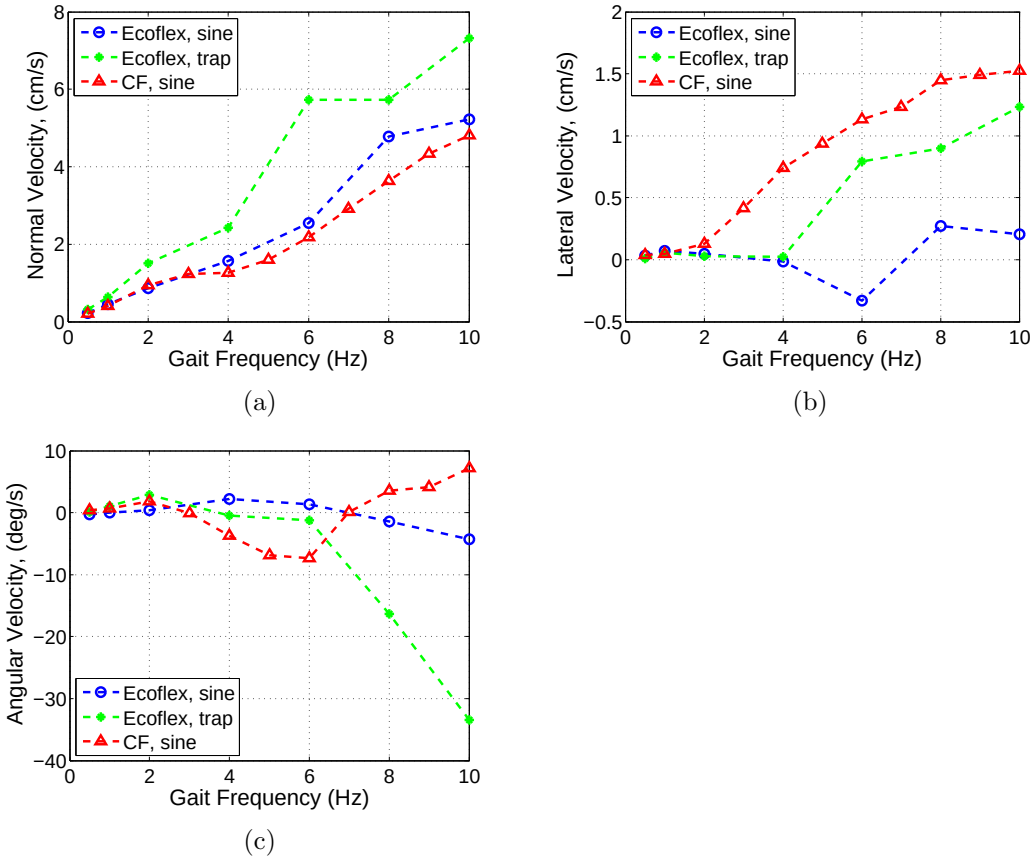

Figure 5.4: HAMR-VP was outfitted with a set of $2mm$ hemisphere molded soft (Shore 0030) silicone rubber (EcoFlex, Smooth-On Inc.) feet. Quasi-static velocity studies were conducted similar to Section 5.2, and comparative results with rigid carbon fiber feet are presented here. Normal velocity using the same 200V sinusoidal inputs remained unchanged between feet (a). However, increased friction enabled the use of higher energy (trapezoidal) waveforms, which increased locomotion speed $17-56\%$ over sinusoidal inputs. Furthermore, increased friction reduced unintended lateral drift (b) and rotation (c) using sinusoidal inputs.

EcoFlex feet, stiction and viscoelasticity prevented locomotion using high gait frequencies; the robot's feet were actuated too quickly to detach from the ground. The results in Section 5.4 with plain carbon fiber feet could possibly be improved with appropriately tuned foot-ground friction, and future work could investigate the effects of friction increased at smaller increments.

5.4 Robot Dynamics

The HAMR powertrain detailed in Chapter 3 benefits from efficient mechanical elements such as bending actuators and flexures with little energy loss (e.g. friction or viscoelasticity). Furthermore, elastic elements in the powertrain (actuator and flexures) and relatively low leg inertia result in system resonance in the high 10s of Hz. This enables the use of gait frequencies that exceed those used in other walking robots. Additionally, a high quality factor leads to increased leg output amplitudes near powertrain resonance. Therefore, in this section, HAMR's powertrain dynamics are characterized and used to increase locomotion speeds and efficiency compared to quasi-static values in Section 5.2.

5.4.1 Full Body Dynamics

A complete system identification of HAMR-VP includes investigating locomotion performance near both powertrain and full body resonances. One could argue that locomotion speed and efficiency might be improved by exciting modes of the dynamic system comprised of the robot (inertia) and powertrain (springs) interacting with the ground; a strategy mentioned in work on DASH [8]. However, in this work only powertrain dynamics were used to enhance locomotion. The primary motivation was an intuition that powertrain resonant frequencies are significantly higher than of the full body dynamic system(s); stiffnesses are comparable in both cases (actuator and flexures), however inertia due to the $1.37g$ robot mass is much greater than a $15mg$ leg. Furthermore, multiple body modes should exist (e.g. bouncing on all four legs, between front and rear, between left and right, and diagonally), not all constructive

to locomotion, with similar frequency responses and therefore difficult to isolate.

To exclude body modes from the discussion of locomotion near powertrain resonance, a simple experiment was performed to approximate full body resonance(s). Resonant frequency of a quadrupedal robot bouncing in the vertical plane, assuming an undamped oscillator, is $f_n = (1/2\pi)\sqrt{k/m}$, where $m = 1.27g$ is the robot mass and k is the combined linear spring stiffness of four parallel powertrains. The stiffness k was estimated by optically measuring sag height in response to incrementally adding weights to the back of the robot. The results in Figure 5.5 show a nearly linear relationship between weight and sag height. A linear fit to the data approximates spring stiffness $k = 5.5N/m$, corresponding to resonant frequency $f_n = 10.4Hz$. f_n represents the maximum body mode resonant frequency; with fewer legs on the ground k, and thus f_n, decrease. Assuming $f_n \leq 10.4Hz$, effects of body mode resonances will be ignored for the analysis near powertrain resonances $(50 - 70Hz)$ below.

5.4.2 Powertrain System Identification

HAMR's powertrain, modeled in Chapter 3, is a second order spring mass system, approximately linear for small leg angles. To characterize the system dynamics, all six robot degrees of freedom (two drive and four lift) were actuated with the robot elevated from the ground at frequencies from $1 - 98Hz$. Sagittal plane outputs were recorded using a high-speed video camera (Phantom v7.3, Vision Research) at 100-3000 fps and measured using 2D motion tracking software (ProAnalyst, Xcitex). Drive and lift DOF amplitudes correspond to horizontal and vertical plane displacements, respectively.

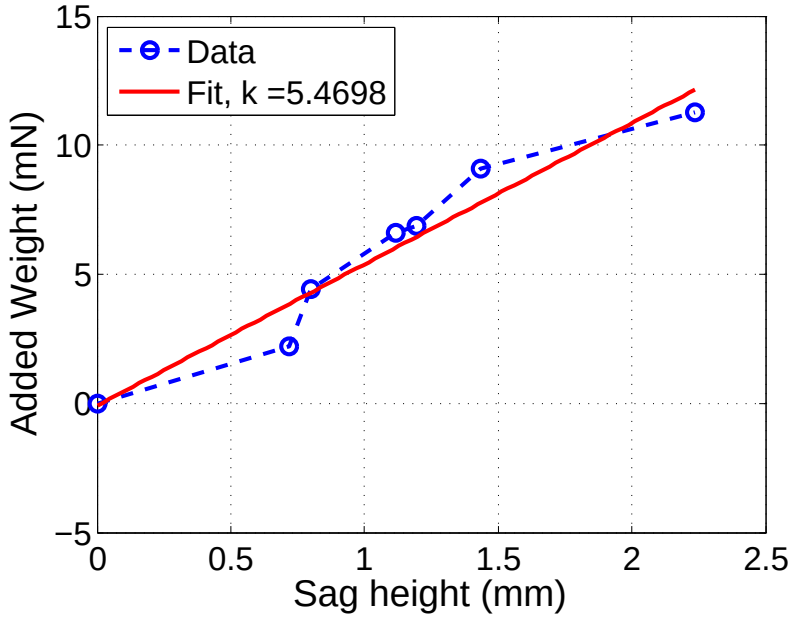

Figure 5.5: The relationship between additional weight and sag height were measured on HAMR-VP to obtain stiffness k and natural frequency $f_n = (1/2\pi)\sqrt{k/m}$ of a four-legged robot of mass m bouncing in the vertical plane.

The robot powertrain frequency responses were recorded using the nominal walking gait described in Figure 5.1; lift and drive DOFs of each leg were actuated 90° out of phase to generate a nominal circular trajectory. Input bias voltage and signal amplitudes were restricted to $100V$ to prevent damage to the powertrains and prolong their lifetime. Figure 5.6 shows system Bode plots with amplitude normalized to the output at $f = 1Hz$ (assumed DC), and phase offset measured between input drive voltage and output displacement. Furthermore, displacement output of independently driven DOFs on HAMR-VP's right side were recorded to identify coupling between lift and drive DOF (see Figure 5.7).

HAMR-VP's powertrains resemble well-behaved linear time invariant second order systems with a high quality factor ($Q = 4.1 - 7.9$). Frequency response data can

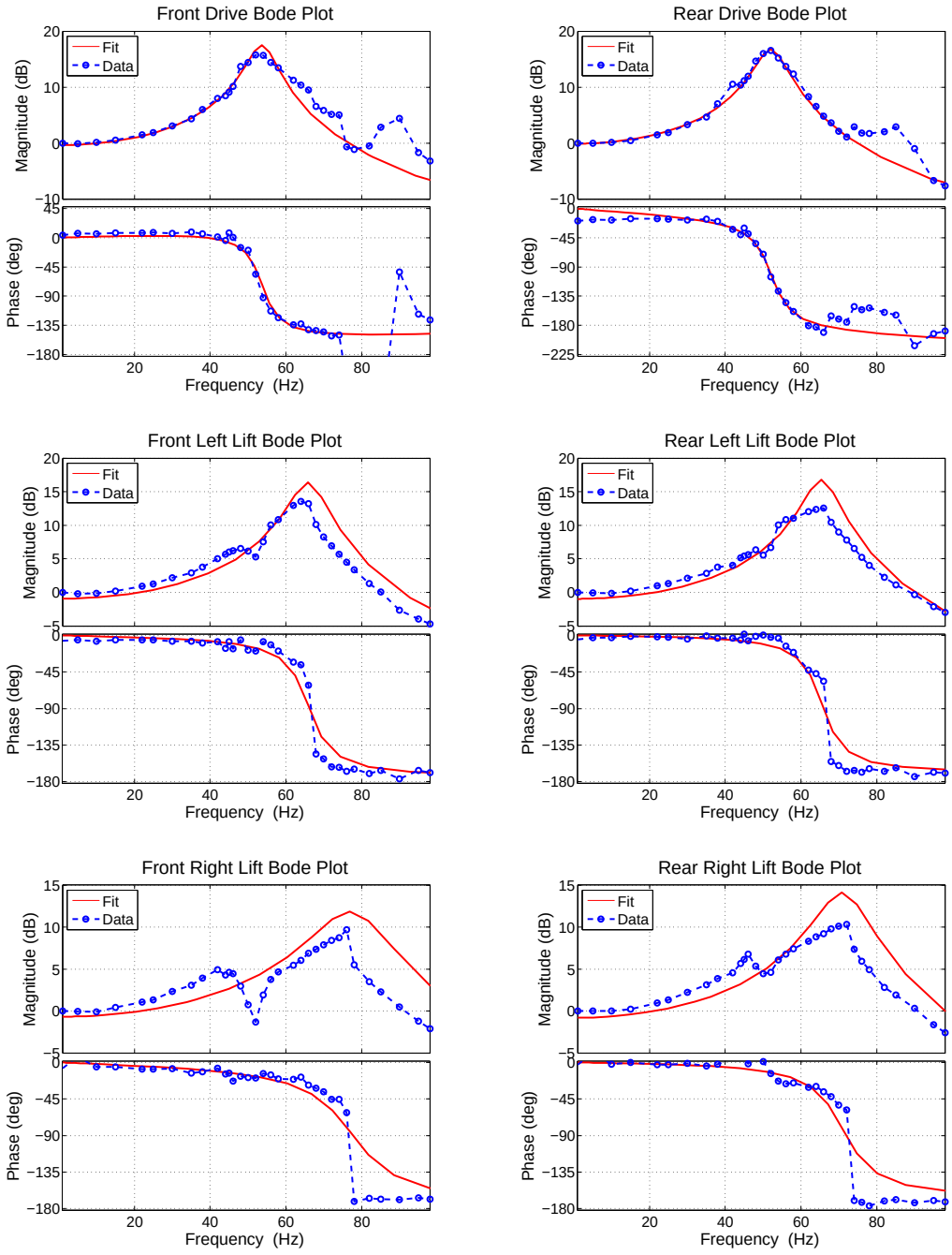

Figure 5.6: Frequency response and second order damped oscillator model fits of HAMR-VP's six DOFs, driven using $100V$ sinusoids and the nominal ψ_i values in Table 5.2.1.

therefore be fit to a damped harmonic oscillator model of the form $\ddot{x}+2\zeta\omega_0\dot{x}+\omega_0^2 x = 0$ where x is a single DOF displacement output, ω_0 is the system natural frequency, and ζ is damping ratio. The system properties of each powertrain obtained from fit models using MATLAB's fitfrd function (2012a, MathWorks) are summarized in Table 5.4.2. Results indicate that all six powertrains are under-damped with damping ratios between 0.063 and 0.122, explaining the robot's quasi-static walking behavior (oscillations causing multiple footfalls per stride) in response to trapezoidal inputs in Section 5.2. Above powertrain resonance, output amplitudes attenuate below values at DC, and phase shifts approach $-180°$. Another observation is the consistency of powertrain dynamic properties, an indication of favorable tolerances using pop-up assembly. This characteristic simplifies control in Section 5.5.

Table 5.2: Dynamic System Properties of the HAMR-VP Powertrain

Powertrain	**Natural Frequency (Hz)**	**Damping Ratio**
Front Drive	54.9	0.063
Rear Drive	51.4	0.073
Front Left Lift	66.2	0.067
Rear Left Lift	65.8	0.063
Front Right Lift	77.8	0.122
Rear Right Lift	71.8	.084

Examining the output of a passive DOF to its driven orthogonal DOF (i.e. actuate lift and measure drive amplitude) identifies coupling near each DOF's resonant frequency; actuating the lift DOF near the drive DOF resonance excites a substantial drive DOF output and vice versa. Additionally, an apparent second resonant frequency of the drive DOF near $90Hz$ only exists when the lift DOF is active, and is therefore related to coupling between the two DOFs. The second drive DOF resonant peak is ignored for this work, and locomotion in Section 5.5 is only performed using

gait frequencies up to $70Hz$.

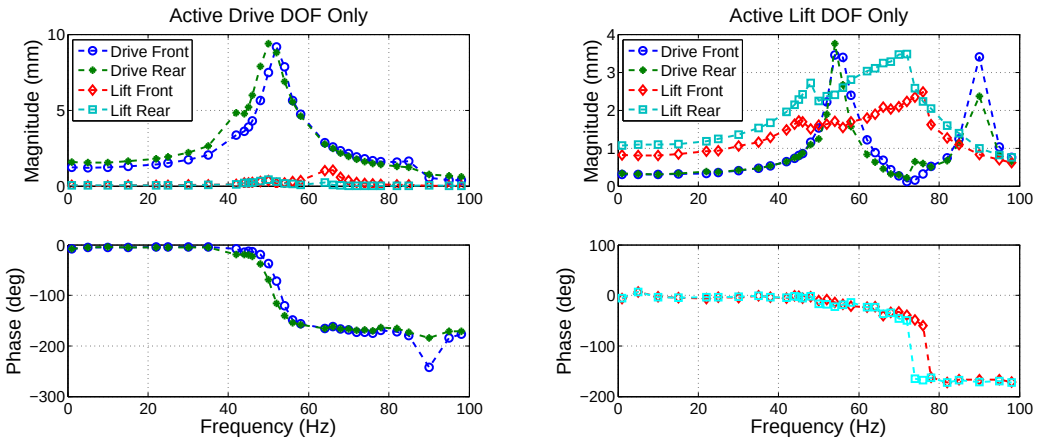

Figure 5.7: Frequency response of HAMR-V's right front (2) and right rear (4) legs with individual DOFs active. The response of passive DOFs when their orthogonal DOF is actuated (e.g. drive output in response to lift input) indicates that there is coupling near passive DOF resonant frequencies. The phenomenon is negligible for the lift DOF in response to drive, however substantial for drive in response to lift.

5.4.3 Tuning Leg Trajectory

Actuating the robot near powertrain resonance amplifies outputs above low frequency values, which in theory increases locomotion efficiency. However, simply driving near powertrain resonant frequencies causes undesirable behavior due to output phase shifts. Using experimental data in the Bode plots in Figure 5.6 and their fit second order systems, appropriate walking trajectories could be generated. Figure 5.8 demonstrates the use of fit second order models to effectively apply a phase shift, α to actuator input signals, creating elliptical foot trajectories. Tuned leg inputs were used to enable high speed locomotion in Section 5.5.

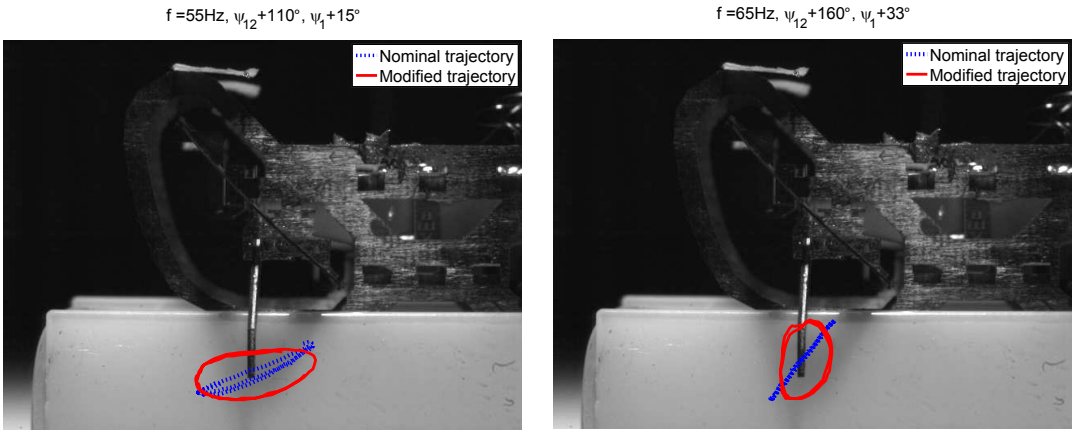

(a) (b)

Figure 5.8: Actuation near powertrain resonant frequencies is susceptible to phase shifts characteristic of a second order linear system. Using the second order system models fit to powertrain frequency response data in Figure 5.6, appropriate phase shifts were applied to input sinusoidal voltages to generate elliptical leg trajectories. Here, results representative of the input tuning process are shown for unmodified and modified outputs of HAMR-VP's front left leg near drive (a) and lift (b) resonances ($55Hz$ and $65Hz$, respectively). Tuned phases are $\alpha_{Li} = 15°, \alpha_{Dr} = 110°$ and $\alpha_{Li} = 33°, \alpha_{Dr} = 160°$ at $55Hz$ and $65Hz$, respectively.

5.5 Exceeding Quasi-Static Locomotion Speeds

Using the powertrain system identification from Section 5.4.2, HAMR-VP was capable of locomotion above the base quasi-static regime in Section 5.2 (1-10Hz). In this section, the robot is nominally fed inputs to generate circular leg trajectories and a trot gait defined in Figure 5.1. The walking surface is card stock, and data is collected using high-speed videography (Phantom v7.3, Vision Research) of the robot sagittal plane combined with overhead video (PL-B741F, Pixelink) of the transverse (walking) plane. Carbon fiber legs were used for all high speed locomotion trials; at frequencies near powertrain resonance, HAMR-VP couldn't lift the sticky, viscoeleastic rubber feet from Section 5.3. Furthermore, exploiting powertrain dynamics requires the

feet to slip and swing freely with respect to the ground. Using intuition gained in Section 5.4.1, full body dynamics are ignored, assuming the maximum system resonance is $10.4Hz$.

In initial trials, HAMR-VP's speed ceased to increase with frequency above $10Hz$; locomotion was characterized by the robot bouncing off of the ground in the vertical direction, slowing or preventing forward motion. Examining the powertrain frequency response data in Figure 5.6 and high speed video of the robot's sagittal plane during locomotion provides and explanation. Above $10Hz$, powertrain output amplitude begins to increase with frequency, and enough lift DOF force is generated to propel the robot off of the ground. When feet leave the ground asymmetrically, one or more strides are missed, altering speed and trajectory. Two solutions exist to this problem: increasing mass or decreasing lift input amplitude; the latter, more energy efficient approach was taken here.

Table 5.3: Tuned Actuator Inputs for Locomotion from $22 - 70Hz$

f (Hz)	V_{a-Li} (V)	V_{a-Dr} (V)	α_{Li} $(^\circ)$	α_{Dr} $(^\circ)$	Max Velocity (cm/s)
22	150	200	0	0	14.2
25	125	200	0	0	14.6
30	125	200	0	0	16.0
35	125	200	0	0	21.5
40	125	200	0	0	26.3
55	120	140	15	110	33.7
60	140	180	25	150	36.0
65	100	200	33	160	36.9
70	110	200	50	167	36.5

Above $40Hz$ gait frequency, in addition to increasing output amplitude, phase shifts caused undesirable leg outputs that altered the direction of locomotion. Using the tuning strategy developed in Section 5.4.3, input phases were adjusted with

a constant phase offset α dictated by second order system fits. From 55-70Hz, leg inputs were tuned to enable HAMR-VP to take advantage of its high quality factor powertrain dynamics. Because of the relatively low variance between each leg's frequency response, a single lift phase and single drive phase offset were chosen for these trials, using leg 1 as the basis. The resulting locomotion was biased to the left, however straight enough to traverse a $17cm \times 17cm$ track without collisions.

Speed results at selected gait frequencies with tuned inputs (summarized in Table 5.5) are shown in Figure 5.9. Velocities at gait frequencies above $22Hz$ are plotted coincident to quasi-static results from Section 5.2, which shows that HAMR-VP exceeds the projected quasi-static maximum. The mechanism enabling greater than quasi-static speeds is inconclusive, however is likely a combination of increased stride amplitudes as dynamics approach resonance, and aerial phases that eliminate quasi-static speed constraints. The maximum speed that HAMR-VP reached in these trials was $36.9cm/s$ (8.4 body lengths per second) and consistently ran at velocities above $30cm/s$ from $55 - 70Hz$ actuator frequencies. See Figure 5.10 for representative frames captured during high speed locomotion.

5.6 Maneuverability

Experiments to determine turning parameters for HAMR-V were conducted in [36] with the help of Dr. Onur Ozcan. The primary goal was to achieve control of body heading in the walking plane (θ) with the simplest possible controller (i.e. fewest parameters) to simplify control for future iterations with onboard electronics. In general, heading can be altered by introducing asymmetry between the output

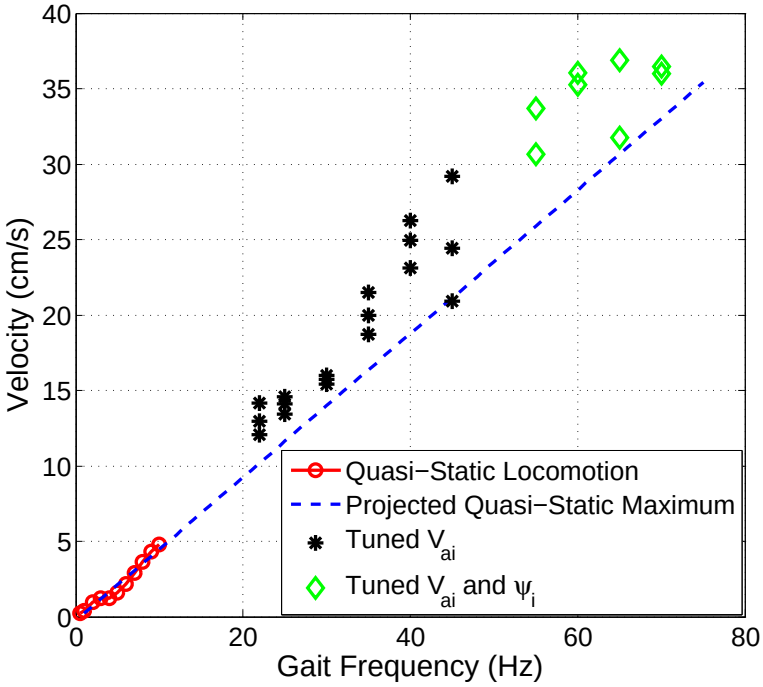

Figure 5.9: High speed locomotion above the $1-10Hz$ quasi-static regime of the HAMR-VP robot was enabled by tuning actuator inputs using the powertrain frequency response data in Section 5.4.2. At gait frequencies from $22-45Hz$, lift DOF voltage amplitudes were attenuated to prevent the robot from bouncing off of the ground, thus disrupting straight line locomotion. From $55-70Hz$, locomotion near powertrain resonances was enabled by attenuating and applying phase shifts to the input voltage (see Table 5.5). Velocities are plotted coincident to quasi-static results and their linear fit, which shows that above 20Hz, speeds exceed the projected quasi-static maximum. Although results are inconclusive, this is likely due to a combination of increased stride amplitudes as dynamics approach resonance and airborne phases that remove speed constraints based on maximum stride length.

amplitudes or frequency of left and right sides of the robot. The robots mechanical coupling of contralateral drive DOFs precludes the use of drive mechanics to generate quasi-static asymmetry between the left and right legs. Therefore, the sagittal plane (lift) DOFs were driven asymmetrically, contrary to the mechanics of turning in insects that primarily occurs in the walking plane [24].

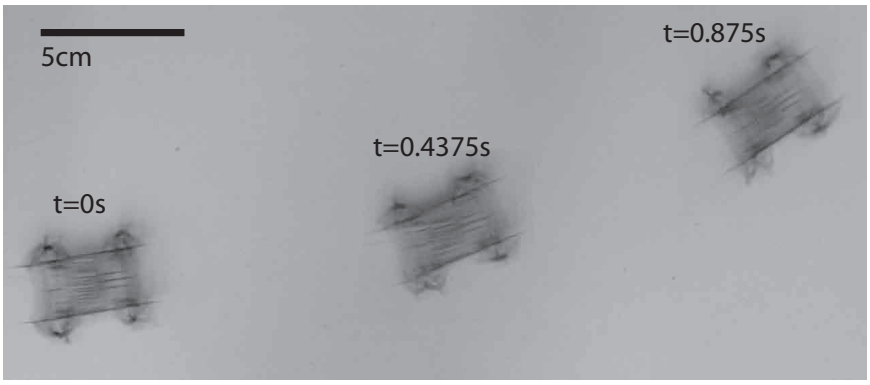

Figure 5.10: HAMR-VP reaches speeds up to $36cm/s$ (8.2 body lengths per second). Shown here is frames captured from locomotion at $36.5cm/s$ using $70Hz$ gait frequency.

5.6.1 Identifying a Simple Maneuverability Control Parameter

A successful orientation control parameter identified in [36] was to introduce an asymmetry between lift DOF phases $\psi_{i=1,2,3,4}$, which were constrained in straight locomotion trials to $\psi_1 = \psi_2 = \psi_3 = \psi_4$. For quasi-static locomotion using carbon fiber feet, varying ψ_i of only a single leg was required to affect HAMR-VP's heading; lateral slipping was required to turn at quasi-static frequencies, precluding the use of soft polymer feet. Results using the lift phase of HAMR-VP's front left leg, ψ_1 for maneuverability are shown in Figure 5.11a.

Dynamic locomotion uses a similar method for turning, however varying ψ_1 only influences left turns. High speed video of the robot's sagittal plane during a turn revealed that varying ψ_i in either direction from the nominal 90° consequently decreases the effective stride length by adding the leg late or removing it early from its stance phase. Therefore, altering ψ_i of two legs is required for bi-directional heading control.

Figure 5.11b illustrates left and right turns controlled by ψ_1 and ψ_2, respectively.

5.6.2 Feedback Control Results

Using the turning scheme presented above, Ozcan developed a feedback controller to demonstrate orientation control in HAMR-V. The controller architecture consisted of low-level code written in MATLAB and Simulink, running on an xPC Target real-time testing environment. Analog drive voltages were output from the xPC Target computer through a DAQ board to high voltage amplifiers. Outputs of $0-200V$ were sent from the amplifiers to HAMR-V's actuators through on-board circuit traces. Sensing was provided by an overhead camera (PL-B741F, Pixelink) to track robot position and orientation. Using the robot state data and a PID controller, HAMR-V's front left lift phase ψ_1 was tuned to reach the desired reference point (see Figure 5.12). In all trials, HAMR-V has a $2Hz$ gait frequency; feedback loop bandwidth limitations precluded higher speed locomotion.

In addition to matching heading, Ozcan developed a feedback loop for trajectory following, which required a second control parameter, lift DOF duty cycle, to account for robot lateral drift; a more significant problem in HAMR-V than HAMR-VP. The resulting 2 DOF controller enabled following straight and sinusoidal trajectories (see Figure 5.13). The effect of duty cycle control on HAMR-VP is yet to be investigated, however lateral drift is smaller and therefore a second control parameter may be unnecessary.

5.7 Discussion

The results in this chapter conclude that by exploting HAMR-VP's high bandwidth and quality factor powertrain dynamics, high speeds above a quasi-static maximum can be reached and at lower input voltages. This study scratched the surface of the potential of HAMR-VP, and much more work can improve locomotion performance. The next steps of this work should be to utilize this strategy to drive HAMR-VP, coincident with proven effective improvements such as tuned foot-ground friction and leg compliance [1].

The HAMR-VP performance is summarized in Table 5.7 alongside earlier prototypes. The chart concludes that the HAMR-VP design is a drastic improvement over earlier prototypes in speed and payload. It should be noted that at high frequencies, HAMR-V has achieved similar speeds to HAMR-VP, however is incapable of supporting sufficient payload for onboard electronics.

Table 5.4: Summarizing HAMR Prototype Results

Robot	**Mass** (g)	**Length** (cm)	**Gait Frequency** (Hz)	**Speed** (cm/s)	**Normalized Speed** (body lengths s^{-1})
HAMR1	0.09	1.7	0-1	< 0.1	< 0.1
HAMR2	2	5.7	0-20	23	4
HAMR3	1.7	4.7	0-20	4.3	0.9
HAMR4	2	5.3	1	0	0
HAMR-V	1.07	3.8	0-60	38	10
HAMR-VP	1.27	4.4	0-70	36.9	8.39

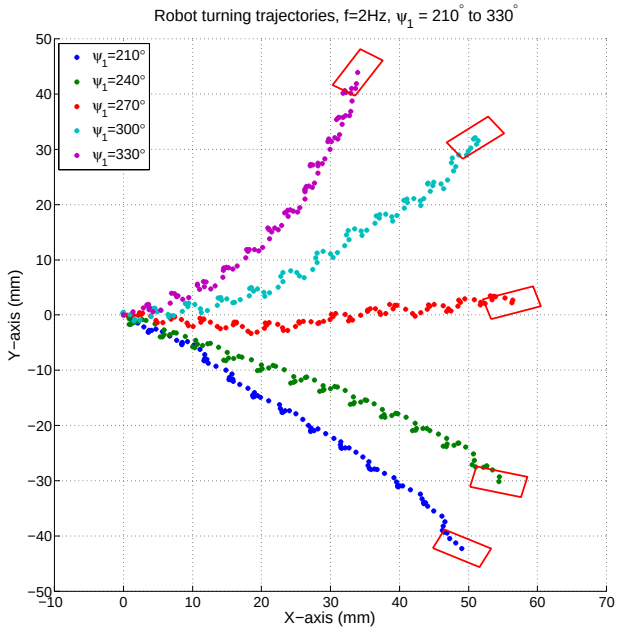

(a)

(b)

Figure 5.11: The orientation of HAMR-V and HAMR-VP can be controlled by altering the phase of lift DOF input signals, ψ_i. Heading during quasi-static operation is controlled by the left front leg's lift phase ψ_1, causing right or left turns by tuning phase from $\psi_1 = 210°$ to $\psi_1 = 330°$, respectively. For dynamic locomotion, two legs are required to affect orientation: ψ_1 for left turns and ψ_2 for right turns (b). In (b) HAMR-V ran at 60Hz gait frequency using $\psi_1 = \psi_2 = 270°$ for nominally straight locomotion (middle), $\psi_1 = 210°, \psi_2 = 270°$ for left turns (bottom), and $\psi_1 = 270°, \psi_2 = 330°$ for right turns (top).

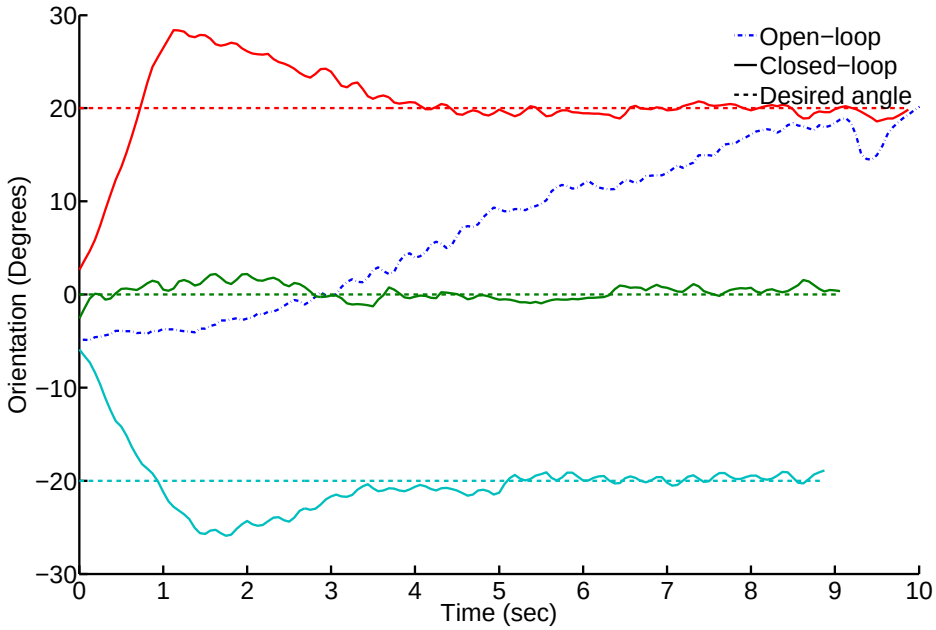

Figure 5.12: An orientation feedback controller for HAMR-V was implemented by Ozcan using ψ_1 as a control parameter for quasi-static locomotion. HAMR-VP's proven ability to use ψ_i for heading control should translate to similar performance.

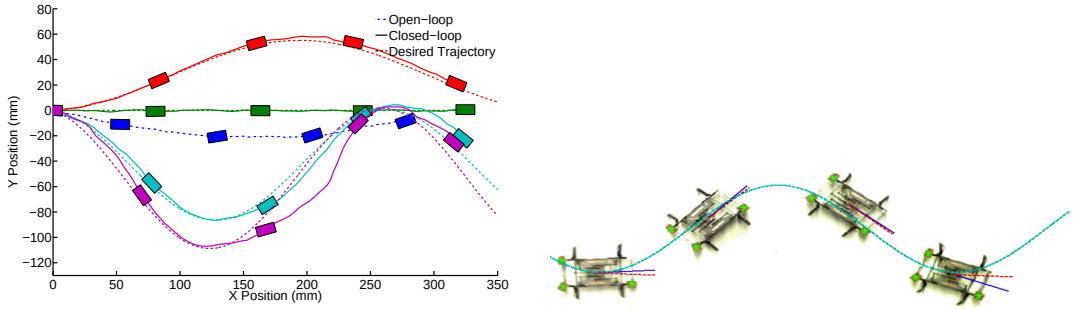

Figure 5.13: A controller was developed to enable HAMR-V to follow trajectories such as sinusoids. A second control parameter, lift DOF duty cycle, was used to affect HAMR-V's lateral velocity. The effect of duty cycle control on HAMR-VP is yet to be investigated.

Chapter 6

Conclusions

Prior to the work in this thesis, the state of the art in insect-scale legged robots was limited to MEMS devices incapable of supporting onboard electronics, and a $2.4g$ robot whose continued development occurred at larger ($> 10g$) scales. A truly at-scale insect-inspired robot had not been conceived capable of high performance locomotion prior to this work.

This thesis contributed designs that combined insect-inspired locomotion, novel high performance mechanisms, and revolutionary manufacturing techniques to enable simple fabrication and high performance locomotion of an insect-inspired walking robot. The Harvard Ambulatory MicroRobot (HAMR) is the first step towards an autonomous, mass-fabricated swarm of intelligent insect-scale terrestrial robots.

In addition to robot designs, the work in this thesis has contributed to manufacturing processes for small-scale mechanisms, and an approach to enabling high speed locomotion in robots with high-bandwidth actuators. Through the development of HAMR, new techniques were developed to improve small-scale laminate ac-

tuator manufacturing, and a method to embed moldable 2.5D soft polymers into PC-MEMS planar devices. In addition, positive locomotion results of the HAMR-VP prototype compared to a hand-assembled alternative concludes that using "pop-up MEMS" manufacturing techniques requires no trade-offs between performance and mechanism complexity.

Due to the direct contributions of this thesis, HAMR has become a platform for testing small-scale electronics, and is a continued platform for legged locomotion research. With a larger payload than other miniature robots such as the RoboBee [32], HAMR has become a platform suitable for testing onboard high voltage power electronics for piezoelectric actuators, sensing, and controls. Current work by Dr. Mike Karpelson includes the implementation of a smaller-scale custom electronics solution than used to power HAMR3, in addition to wireless powering solutions to enable an experimental test platform without the use of rechargeable batteries. Furthermore, work by Dr. Onur Ozcan is addressing onboard sensing and control for HAMR, including the use of MEMS-based inertial measurement units and optical flow sensors.

The HAMR-VP platform, although capable of impressive locomotion performance, has only been tested on flat ground in an ideal laboratory setting. A significant amount of work is required to bring the goal of an autonomous swarm of robots to fruition. A relatively low hanging fruit is achieving a fully monolithic HAMR design to eliminate all manual assembly steps and enable mass production. In the design of HAMR-VP, actuators, circuit boards, and legs were intentionally modular due to concurrent work. However, recent improvements in piezoelectric actuator designs has increased robustness to failure; the final HAMR-VP used these actuators without

failure for greater than 10^5 cycles, on the same order of magnitude as flexure lifetime. Furthermore, designs for onboard electronics are near completion, and if proven capable of driving HAMR-VP, could be implemented into a monolithic manufacturing process using PC-MEMS.

Leg and foot mechanics are still important areas of study and will be continued to examine their effects on locomotion. The manufacturing process presented in this work for PC-MEMS components embedded with moldable soft polymers is a tool to generate designs with varying leg dynamic properties and feet that affect ground locomotion efficiency, robustness to shocks, and ability to climb obstacles. With additional work in these areas, the dream of developing a swarm of autonomous insect-scale terrestrial robots for hazardous environment sensing is achievable.

Bibliography

[1] R.M. Alexander. Three uses for springs in legged locomotion. *The Intl. J. of Robotics Research*, 9(2):53–61, 1990.

[2] T.J. Allen, R.D. Quinn, R. Bachman, and R.E. Ritzmann. Whegs ii: A mobile robot using abstracted biological principles. In *IEEE/RSJ Intl. Conf. on Intelligent Robots and Systems*, Sendai, Japan, 2004.

[3] A. Asbeck, S. Dastoor, A. Parness, L. Fullerton, N. Esparza, D. Soto, B. Heyneman, and M. Cutkosky. Climbing rough vertical surfaces with hierarchical directional adhesion. In *IEEE Intl. Conf. on Robotics and Automation*, pages 2675–2680, Kobe, Japan, 2009.

[4] S. Avadhanula and R.S. Fearing. Flexure design rules for carbon fiber microrobotic mechanisms. In *IEEE Intl. Conf. on Robotics and Automation*, pages 1579–1584. IEEE, 2005.

[5] A.T. Baisch, C. Heimlich, M. Karpelson, and R.J. Wood. HAMR3: An autonomous 1.7g ambulatory robot. In *IEEE/RSJ Intl. Conf. on Intelligent Robots and Systems*, pages 5073–5079, San Francisco, CA. USA, 2011.

[6] P. Birkmeyer, A.G. Gillies, and R.S. Fearing. Clash: Climbing vertical loose cloth. In *IEEE/RSJ Intl. Conf. on Intelligent Robots and Systems*, pages 5087–5093, San Francisco, CA, 2011.

[7] P. Birkmeyer, A.G. Gillies, and R.S. Fearing. Dynamic climbing of near-vertical smooth surfaces. In *IEEE/RSJ Intl. Conf. on Intelligent Robots and Systems*, Vilamoura, Portugal, 2012.

[8] P. Birkmeyer, K. Peterson, and R.S. Fearing. DASH: A dynamic 16g hexapedal robot. In *IEEE/RSJ Intl. Conf. on Intelligent Robots and Systems*, pages 2683–2689, St. Louis, MO, 2009.

[9] D. Campolo, R. Sahai, and R.S. Fearing. Development of piezoelectric bending actuators with embedded piezoelectric sensors for micromechanical flapping mechanisms. In *IEEE Intl. Conf. on Robotics and Automation*, volume 3, pages 3339–3346. IEEE, 2003.

[10] J.G. Cham, S.A. Bailey, J.E. Clark, R.J. Full, and M.R. Cutkosky. Fast and robust: Hexapedal robots via shape deposition manufacturing. *The Intl. J. of Robotics Research*, 21(10-11):869–882, 2002.

[11] Boston Dynamics. CHEETAH - Fastest Legged Robot. `http://www.bostondynamics.com/robot_cheetah.html`, 2013. [Online; accessed 26-March-2013].

[12] T. Ebefors, J.U. Mattsson, E. Kälvesten, and G. Stemme. A walking silicon micro-robot. In *Proc. Transducers*, pages 1202–1205. Citeseer, 1999.

[13] R.J. Full and D.E. Koditschek. Templates and anchors: neuromechanical hypotheses of legged locomotion on land. *J. of Experimental Biology*, 202(23):3325–3332, 1999.

[14] R.J. Full, T. Kubow, J. Schmitt, P. Holmes, and D. Koditschek. Quantifying dynamic stability and maneuverability in legged locomotion. *Integrative and comparative biology*, 42(1):149–157, 2002.

[15] R.J. Full and M.S. Tu. Mechanics of a rapid running insect: two-, four- and six-legged locomotion. *J. of Experimental Biology*, 156:215–231, 1991.

[16] D.I. Goldman, T.S. Chen, and D.M. Dudek. Dynamics of rapid vertical climbing in cockroaches reveals a template. *J. of Experimental Biology*, 209(15):2990, 2006.

[17] D.W Haldane, K.C. Peterson, F.L. Garcia Bermudez, and R.S. Fearing. Animal-inspired design and aerodynamic stabilization of a hexapedal millirobot. In *IEEE Intl. Conf. on Robotics and Automation*, Karlsruhe, Germany, 2013.

[18] M. Heckele and W.K. Schomburg. Review on micro molding of thermoplastic polymers. *J. of Micromechanics and Microengineering*, 14(3):R1, 2004.

[19] C. Heimlich. Embedded control for a crawling robotic insect. Master's thesis, Ecole Polytechnique Federale de Lausanne, 2010.

[20] K.L. Hoffman and R.J. Wood. Turning gaits and optimal undulatory gaits for a modular centipede-inspired millirobot. In *4th IEEE RAS/EMBS Conf. on Biomedical Robotics and Biomechatronics (BioRob)*, pages 1052–1059, Rome, Italy, 2012.

[21] S. Hollar, A. Flynn, C. Bellew, and K.S.J. Pister. Solar powered 10 mg silicon robot. In *IEEE Intl. Conf. on Micro Electro Mechanical Systems (MEMS)*, pages 706–711. IEEE, 2003.

[22] A. Hoover, E. Steltz, and R.S. Fearing. Roach: An autonomous 2.4g crawling hexapod robot. In *IEEE/RSJ Intl. Conf. on Intelligent Robots and Systems*, Nice, France, 2008.

[23] P.E. Hudson, S.A. Corr, R.C. Payne-Davis, S.N. Clancy, E. Lane, and M.A. Wilson. Functional anatomy of the cheetah (acinonyx jubatus) hindlimb. *J. of anatomy*, 218(4):363–374, 2011.

[24] D.L. Jindrich and R.J. Full. Many-legged maneuverability: dynamics of turning in hexapods. *J. of Experimental Biology*, 202(12):1603–1623, 1999.

[25] M. Karpelson, G.-Y. Wei, and R.J. Wood. Driving high voltage piezoelectric actuators in microrobotics applications. *J. Sensors and Actuators A: Physical*, 176:78–89, 2012.

[26] M. Karpelson, G.Y. Wei, and R.J. Wood. Milligram-scale high-voltage power electronics for piezoelectric microrobots. In *IEEE Intl. Conf. on Robotics and Automation*, Kobe, Japan, 2009.

[27] S. Kim, J.E. Clark, and M.R. Cutkosky. iSprawl: Design and tuning for high-speed autonomous open-loop running. *Intl. J. of Robotics Research*, 25(9):903–912, 2006.

[28] S. Kim, M. Spenko, S. Trujillo, B. Heyneman, D. Santos, and M.R. Cutkosky. Smooth vertical surface climbing with directional adhesion. *IEEE Transactions on Robotics*, 24(1):65–74, 2008.

[29] J. Lee and R.S. Fearing. Wet self-cleaning of superhydrophobic microfiber adhesives formed from high density polyethylene. *Langmuir*, 28(43):15372–15377, 2012.

[30] C. Li, A.M. Hoover, P. Birkmeyer, P.B. Umbanhowar, R.S. Fearing, and D.I. Goldman. Systematic study of the performance of small robots on controlled laboratory substrates. In *SPIE Defense, Security, and Sensing Conf.*, Orlando, FL, April 2010.

[31] C. Li, P.B. Umbanhowar, H. Komsuoglu, D.E. Koditschek, and D.I. Goldman. Sensitive dependence of the motion of a legged robot on granular media. *Proc. of the National Academy of Sciences*, 106(9):3029–3034, 2009.

[32] K.Y. Ma, S.M. Felton, and R.J. Wood. Design, fabrication, and modeling of the split actuator microrobotic bee. In *IEEE/RSJ Intl. Conf. on Intelligent Robots and Systems*, pages 1133–1140. IEEE, 2012.

[33] Y. Mengüç, S.Y. Yang, S. Kim, J. Rogers, and M. Sitti. Gecko-inspired controllable adhesive structures applied to micromanipulation. *Advanced Functional Materials*, 22(6):1246–1254, 2012.

[34] M.P.Murphy, C. Kute, Y. Mengüç, and M. Sitti. Waalbot ii: Adhesion recovery and improved performance of a climbing robot using fibrillar adhesives. *The Intl. J. of Robotics Research*, 30(1):118–133, 2011.

[35] K. Otsuka and C.M. Wayman. *Shape memory materials*. Cambridge University Press, 1999.

[36] O. Ozcan, A.T. Baisch, and R.J. Wood. Design and feedback control of a biologically inspired miniature quadruped. In review: *IEEE Intl. Conf. on Robotics and Automation*, Tokyo, Japan, 2013.

[37] A.O. Pullin, N.J. Kohut, D. Zarrouk, and R.S. Fearing. Dynamic turning of 13 cm robot comparing tail and differential drive. In *IEEE Intl. Conf. on Robotics and Automation*, pages 5086–5093. IEEE, 2012.

[38] M.H. Raibert. *Legged robots that balance*. The MIT Press, Cambridge, MA, 1985.

[39] R R.M. Alexander. Tendon elasticity and muscle function. *Comparative Biochemistry and Physiology-Part A: Molecular & Integrative Physiology*, 133(4):1001–1011, 2002.

[40] U. Saranli, M. Buehler, and D.E. Koditschek. RHex - a simple and highly mobile hexapod robot. *Intl. J. of Robotics Research*, 20:616–631, July 2001.

[41] M.J. Spenko, G.C. Haynes, J.A. Saunders, M.R. Cutkosky, A.A. Rizzi, R.J. Full, and D.E. Koditschek. Biologically inspired climbing with a hexapedal robot. *J. of Field Robotics*, 25(4-5):223–242, 2008.

[42] S. Sponberg and R.J. Full. Neuromechanical response of musculo-skeletal structures in cockroaches during rapid running on rough terrain. *J. of Experimental Biology*, 211:433–446, May 2008.

[43] P.S. Sreetharan, J.P. Whitney, M.D. Strauss, and R.J. Wood. Monolithic fabrication of millimeter-scale machines. *J. of Micromechanics and Microengineering*, 22(5):055027, 2012.

[44] Z.E. Teoh and R.J. Wood. A flapping-fing microrobot with a differential angle-of-attack mechanism. In *IEEE Intl. Conf. on Robotics and Automation*, Karlsruhe, Germany, 2013.

[45] W.S.N. Trimmer. Microrobots and micromechanical systems. *Sensors and actuators*, 19(3):267–287, 1989.

[46] K.J. Waldron and G.L. Kinzel. *Kinematics, dynamics, and design of machinery*. Wiley, 2004.

[47] J.P. Whitney, P.S. Sreetharan, K.Y. Ma, and R.J. Wood. Pop-up book mems. *J. of Micromechanics and Microengineering*, 21(11):115021, 2011.

[48] R.J. Wood. The first flight of a biologically-inspired at-scale robotic insect. *IEEE Transactions on Robotics*, 24(2), April 2008.

[49] R.J. Wood. The first takeoff of a biologically inspired at-scale robotic insect. *IEEE Transactions on Robotics*, 24(2):341–347, 2008.

[50] R.J. Wood, S. Avadhanula, R. Sahai, E. Steltz, and R.S. Fearing. Microrobot design using fiber reinforced composites. *J. of Mechanical Design*, 130:052304, 2008.

[51] R.J. Wood, E. Steltz, and R.S. Fearing. Optimal energy density piezoelectric bending actuators. *J. of Sensors and Actuators A: Physical*, 119(2):476–488, 2005.

[52] Y. Xia and G.M. Whitesides. Soft lithography. *Annual Review of Materials Science*, 28(1):153–184, 1998.

[53] J. Yan, R.J. Wood, S. Avadhanula, M. Sitti, and R.S. Fearing. Towards flapping wing control for a micromechanical flying insect. In *IEEE Intl. Conf. on Robotics and Automation*, volume 4, pages 3901–3908. IEEE, 2001.

[54] X. Zhou and S. Bi. A survey of bio-inspired compliant legged robot designs. *Bioinspiration & biomimetics*, 7(4):041001, 2012.

Appendix A

HAMR Lift DOF Powertrain Model Derivation

The HAMR powertrain consists of a single 2 DOF spherical five-bar hip joint, defining the lift and drive DOFs of a single leg. Each input to the SFB is driven by a piezoelectric bending actuator, with displacement amplified by a four-bar flexure-based transmission. Using the assumption that SFB outputs are largely decoupled, the HAMR powertrain can be modeled as two single DOF systems, each consisting of an actuator, four-bar transmission, and leg (see Figure A.1).

Actuators are modeled as a force source, F_{act} in parallel with a linear spring with stiffness k_{act} and tip displacement δ_{act}. Actuator resonance is assumed on the order of 1KHz, well above the stride frequencies (1-70Hz) used in HAMR. The actuator is therefore operating quasi-statically and its mass is ignored. A serial compliance, k_{ser} is included between the actuator output and transmission input to represent compliance observed in the robot due to a non-rigid exoskeleton and off-axis flexure bending

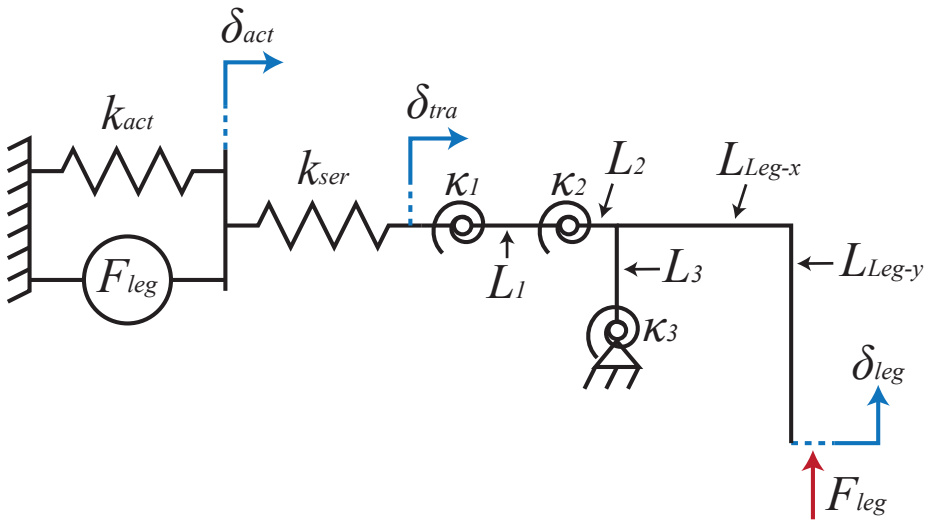

Figure A.1: Single degree of freedom model of the HAMR lift DOF powertrain. An actuator, modeled as a force source in parallel with compliance k_{act}, drives a four-bar flexure-based transmission with torsional stiffness κ_i and link lengths L_j to impart a blocked force or displacement at the tip of a leg. A serial spring stiffness k_{ser} represents non-ideal characteristics of the robot such as exoskeleton and flexure off-axis compliance (twisting and buckling).

(buckling and twisting). The four-bar transmission takes an input displacement δ_{tra} and has rigid, massless links with lengths $L_{j=1,2,3}$. Flexures in the four-bar transmission are modeled as ideal pin joints with angular displacement ϕ_i and a linear torsional spring with stiffness κ_i $(i = 1, 2, 3)$. A pin joint approximation is satisfied by the casselated flexure design described in Section 3.2. Legs are modeled as a rigid, massless extension from the four-bar transmission output with horizontal and vertical dimensions L_{Leg-x} and L_{Leg-y}, respectively. The entire system model is lossless; a system ID in Chapter 5 confirms that the powertrain behaves like an under-damped 2nd-order system with damping ratio between $0.06 - 0.12$.

Assuming all stiffness values and linkage lengths are known, the system has a single degree of freedom. The displacement of the actuator can be directly mapped

to the displacement of the leg. Writing a power balance yields:

$$F_{\text{act}}\frac{\partial \delta_{\text{act}}}{\partial t} - k_{\text{act}}\delta_{\text{act}}\frac{\partial \delta_{\text{act}}}{\partial t} + k_{\text{ser}}(\delta_{\text{tra}} - \delta_{\text{act}})\frac{\partial \delta_{\text{act}}}{\partial t} \ldots \\ - k_{\text{ser}}(\delta_{\text{tra}} - \delta_{\text{act}})\frac{\partial \delta_{\text{tra}}}{\partial t} + \kappa_1\Phi_1\frac{\partial \Phi_1}{\partial t} + \kappa_2\phi_2\frac{\partial \Phi_2}{\partial t} \ldots \\ + \kappa_3\Phi_3\frac{\partial \Phi_3}{\partial t} - F_{\text{leg}}\frac{\partial \delta_{\text{leg}}}{\partial t} = 0, \quad \text{(A.1)}$$

Transmission flexures are assumed to behave like ideal pin joints with no damping, which means that δ_{tra} can be directly mapped to δ_{leg}, yielding the following force balance:

$$F_{act} = k_{act}\delta_{act} = k_{ser}(\delta_{tra} - \delta_{act}), \quad \text{(A.2)}$$

which yields:

$$\frac{\partial \delta_{\text{act}}}{\partial \delta_{\text{tra}}} = \frac{1}{1 + \frac{k_{\text{act}}}{k_{\text{ser}}}} = A. \quad \text{(A.3)}$$

The term A governs the ratio of actuator deflection δ_{act} lost due to imperfections to that transmitted through the transmission as δ_{tra}. As $k_{ser} \to 0$, i.e. the imperfections dominate the entire behavior of the powertrain, $A \to 0$, which means none of the actuator deflection will be imparted on the transmission. As $k_{ser} \to \infty$, i.e. no imperfections, $A \to 1$, which means all of the actuator deflection will be imparted to the transmission. Dividing Equation (A.1) with $\partial \delta_{\text{tra}}/\partial t$ and substituting Equation (A.3) in Equation (A.1) yields:

$$AF_{\text{act}} - Ak_{\text{act}}\delta_{\text{tra}} + \kappa_1\Phi_1\frac{\partial\Phi_1}{\partial\delta_{\text{tra}}} + \kappa_2\phi_2\frac{\partial\Phi_2}{\partial\delta_{\text{tra}}}\ldots$$
$$+ \kappa_3\Phi_3\frac{\partial\Phi_3}{\partial\delta_{\text{tra}}} - F_{\text{leg}}R_{\text{tra}} = 0, \quad \text{(A.4)}$$

where $R_{\text{tra}} = \partial\delta_{\text{leg}}/\partial\delta_{\text{tra}}$ is the relative movement of the leg with respect to the movement of the transmission input; hence it is the instantaneous transmission ratio. The terms $\frac{\partial\Phi_1}{\partial\delta_{\text{tra}}}$, $\frac{\partial\Phi_2}{\partial\delta_{\text{tra}}}$, $\frac{\partial\Phi_3}{\partial\delta_{\text{tra}}}$, R_{tra} and δ_{tra} can be solved kinematically for a given leg displacement and the force experienced by the leg can be found with known stiffness and transmission geometric parameters, and modeled or experimental actuator outputs. The full equation can be solved numerically using MATLAB's fsolve function.